World Energy Demand

2100: 40-50 TW
2050: 25-30 TW

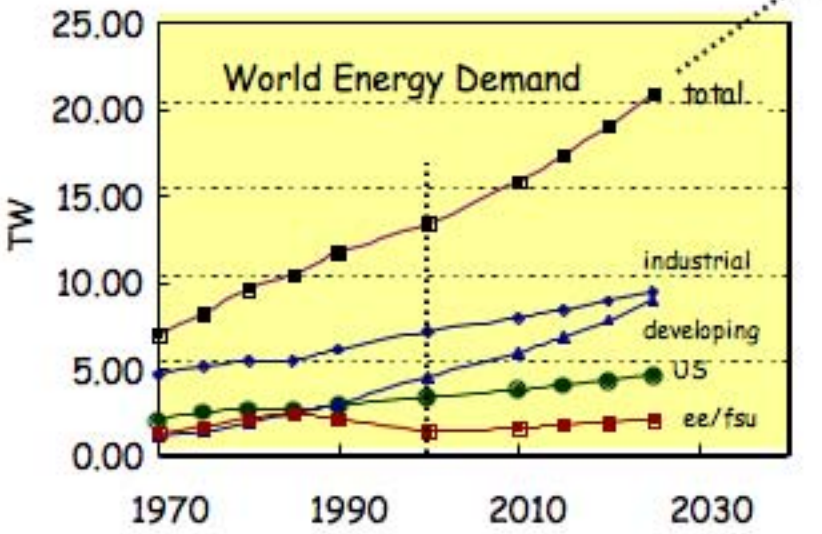

energy gap
~ 14 TW by 2050
~ 33 TW by 2100

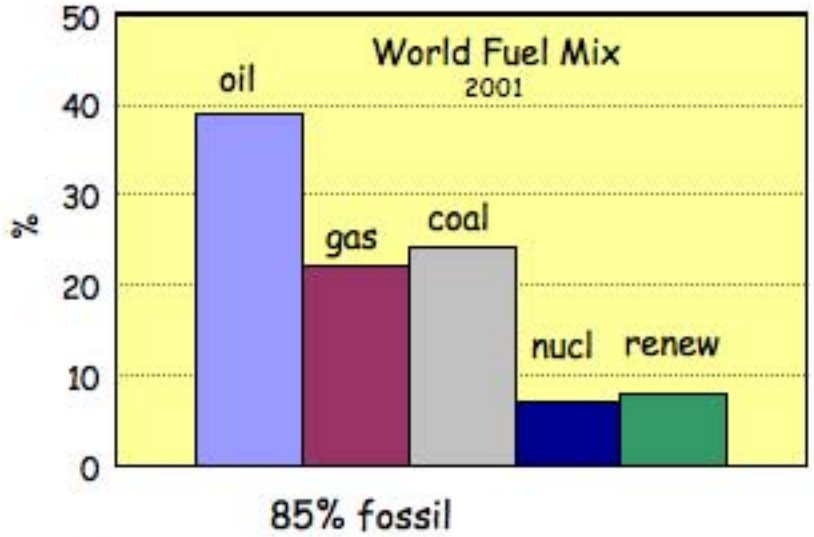

85% fossil

EIA Intl Energy Outlook 2004
http://www.eia.doe.gov/oiaf/ieo/index.html

Hoffert et al Nature 395, 883,1998

Fossil: Climate Change

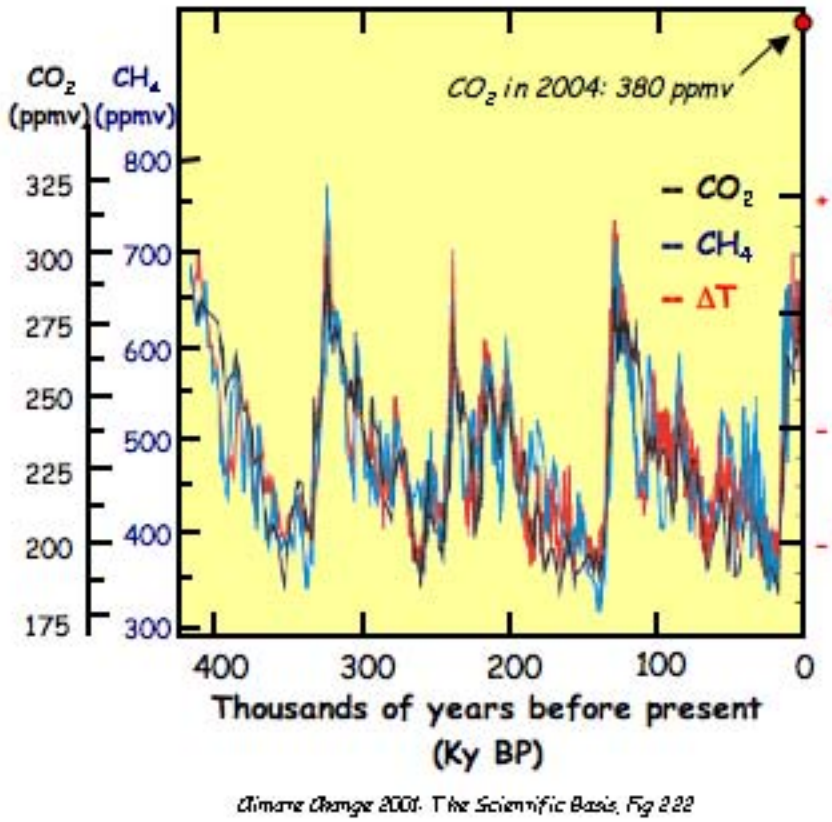

Climate Change 2001: The Scientific Basis, Fig 2.22

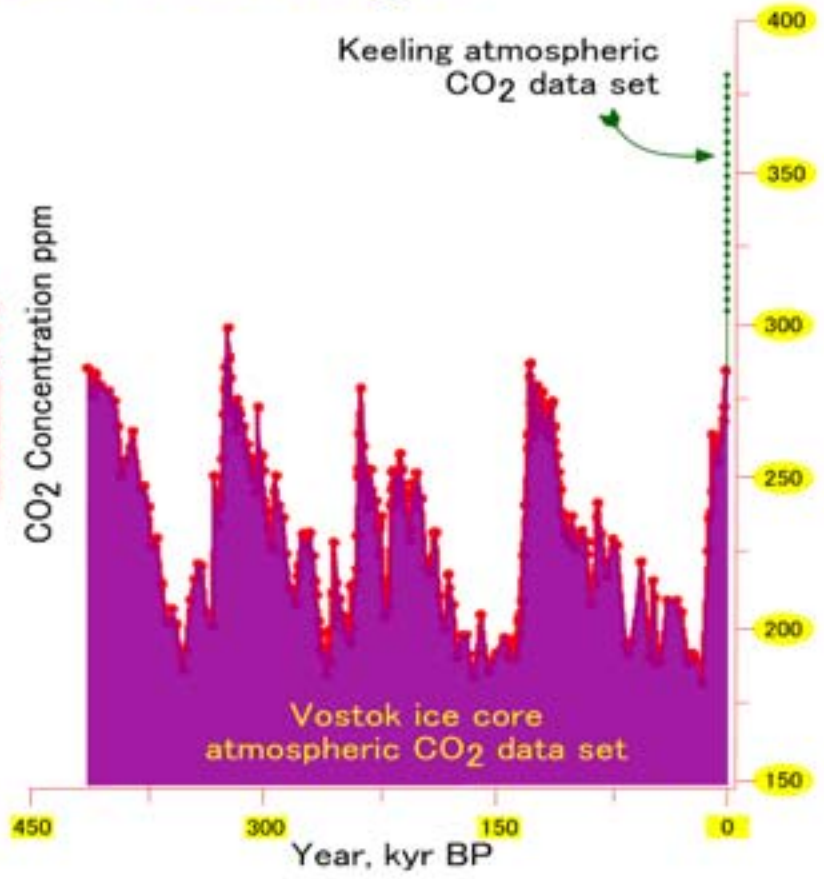

Intergovernmental Panel on Climate Change, 2001
http://www.ipcc.ch
N. Oreskes, Science **306**, 1686, 2004
D. A. Stainforth et al, Nature **433**, 403, 2005

Relaxation time

transport of CO_2 or heat to deep ocean: >3000 years

The Energy Gap

- ~ 14 TW of additional power by 2050
- ~ 33 TW of additional power by 2100

2004 capacity: 13 TW

fossil energy

after oil production peaks, switch to gas and coal

capture/store 22 Gtonnes of CO_2/yr (current emissions)

- 12,500 km^3 at atmospheric pressure = volume of Lake Superior
- 600 times CO_2 injected in oil wells/yr to spur production
- 100 times the natural gas drawn in and out of geologic storage/yr to smooth demand
- 20,000 times CO_2 stored/yr in Norway's Sleipner offshore reservior
- ~~no leaks: 1% leak rate nullifies storage in 100 yrs~~

nuclear energy

14,000 1 GW_e fission reactors - 1 new reactor/day for 38 years

Renewable Energy

Solar

1.2×10^5 TW at Earth surface

600 TW practical

energy gap
~ 14 TW by 2050
~ 33 TW by 2100

Wind

2-4 TW extractable

Biomass

5-7 TW gross
all cultivatable
land not used
for food

Tide/Ocean Currents

2 TW gross

Hydroelectric

4.6 TW gross
1.6 TW technically feasible
0.9 TW economically feasible
0.6 TW installed capacity

Geothermal

12 TW gross over land
small fraction recoverable

Energy Conversion Strategies

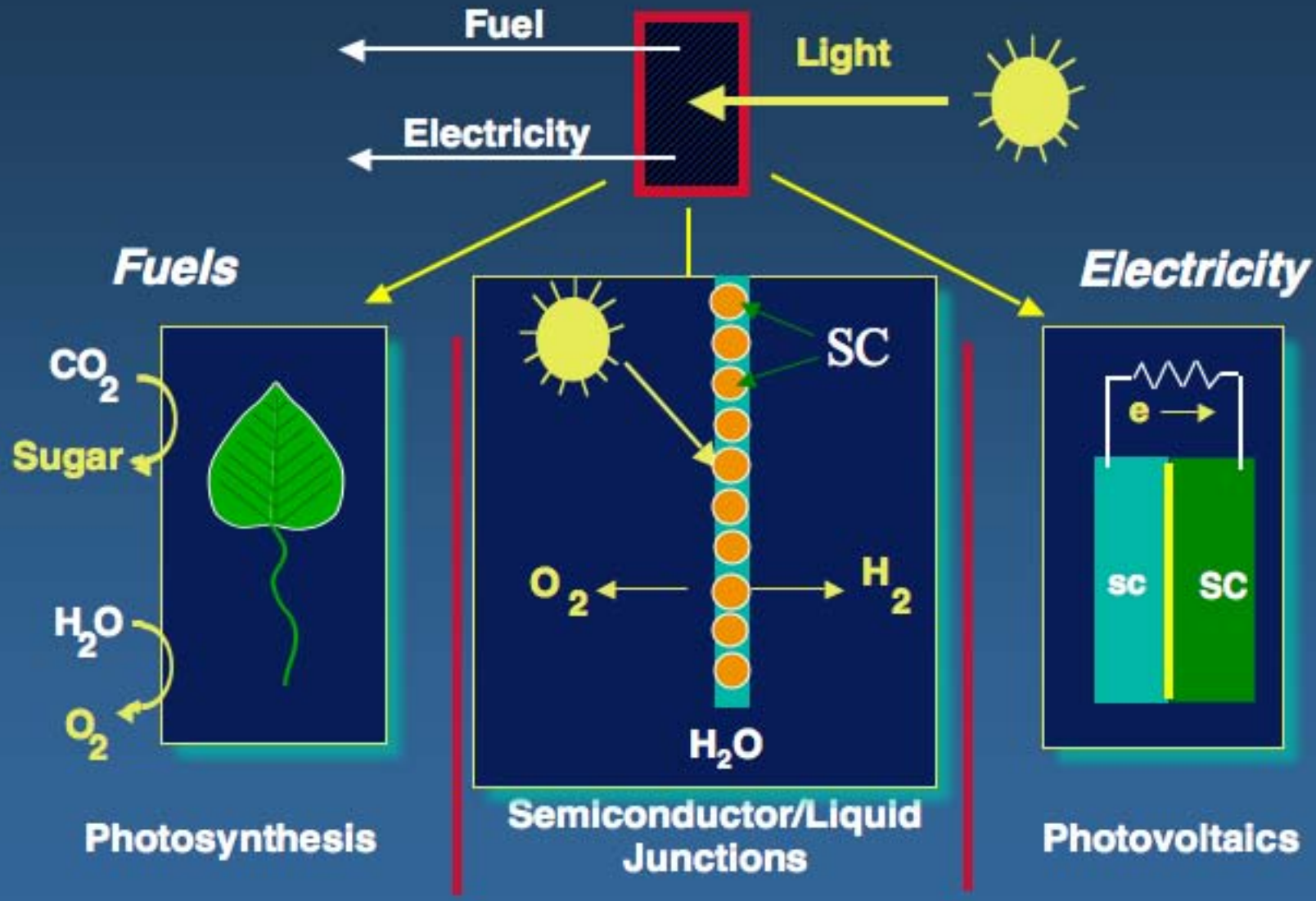

TABLE 5.14. CURRENT GLOBAL LAND-USE PATTERN

Cropland (arableland and permanent crops)		Forests and woodland		Permanent pastures		Other land		
						Total other land		Land with rainfed cultivation potential
Gha	% of total	Gha	% of total	Gha	% of total	Gha	% of total	Gha
1.5	11	4.2	21	3.4	26	4.0	31	1.6–1.8

Note: Gha stands for billions of hectares. Total land availability is 13.1 billion hectares.

Source: FAO, 1995, 1999; Fischer and Heilig, 1998; WRI, 1998.

TABLE 5.15. PROJECTED BIOMASS ENERGY POTENTIAL, 2050 (BILLIONS OF HECTARES UNLESS OTHERWISE INDICATED)

1	2	3	4	5	6[a]	7[b]	7[c]
Region	Population in 2050 (billions)	Land with crop production potential in 1990	Cultivated land in 1990	Additional cultivated land required in 2050	Maximum additional area for biomass production	Maximum additional amount of energy from biomass (exajoules)	
Industrialised countries[d]	–	–	0.670	0.050	0.100	17	30
Latin America							
Central and Caribbean	0.266	0.087	0.037	0.015	0.035	6	11
South America	0.524	0.865	0.153	0.082	0.630	107	189
Africa							
East	0.698	0.251	0.063	0.068	0.120	20	36
Central	0.284	0.383	0.043	0.052	0.288	49	86
North	0.317	0.104	0.040	0.014	0.050	9	15
Southern	0.106	0.044	0.016	0.012	0.016	3	5
West	0.639	0.196	0.090	0.096	0.010	2	3
Asia (excl. China)							
Western	0.387	0.042	0.037	0.010	-0.005	0	0
South-central	2.521	0.200	0.205	0.021	-0.026	0	0
East	1.722	0.175	0.131	0.008	0.036	6	11
South-east	0.812	0.148	0.082	0.038	0.028	5	8
China	–	–	–	–	–	2[e]	2[e]
Total[f]	**8.295**	**2.495**	**0.897**	**0.416**	**1.28**	**226**	**396**
Global biomass energy potential						**276[g]**	**446[g]**

a. (6) = (3) – (4) – (5). b. (7) = (6) x 8.5 [oven dry tonnes a hectare per year] x 20 [GJ per oven dry tonne] based on higher heating value (18 GJ per oven dry tonne for lower heating value). The assumptions for biomass productivity may appear on the high side, but they represent technically achievable yields given dedicated research, development, and dissemination. c. (7) = (6) x 15 [oven dry tonnes a hectare per year] x 20 [GJ per oven dry tonne] based on higher heating value (18 GJ per oven dry tonne for lower heating value). d. OECD, Central and Eastern Europe, newly independent states of the former Soviet Union. e. Data are projected values from d'Apote (1998), not maximum estimates. f. Totals in (2), (3), (4), and (5) exclude industrialised countries. g. Includes 50 EJ of current biomass energy generation.

Source: Derived from Fischer and Heilig, 1998; d'Apote, 1998; Nakicenovic, Grübler, and McDonald, 1998.

Bacterial Photosynthetic Reaction Center

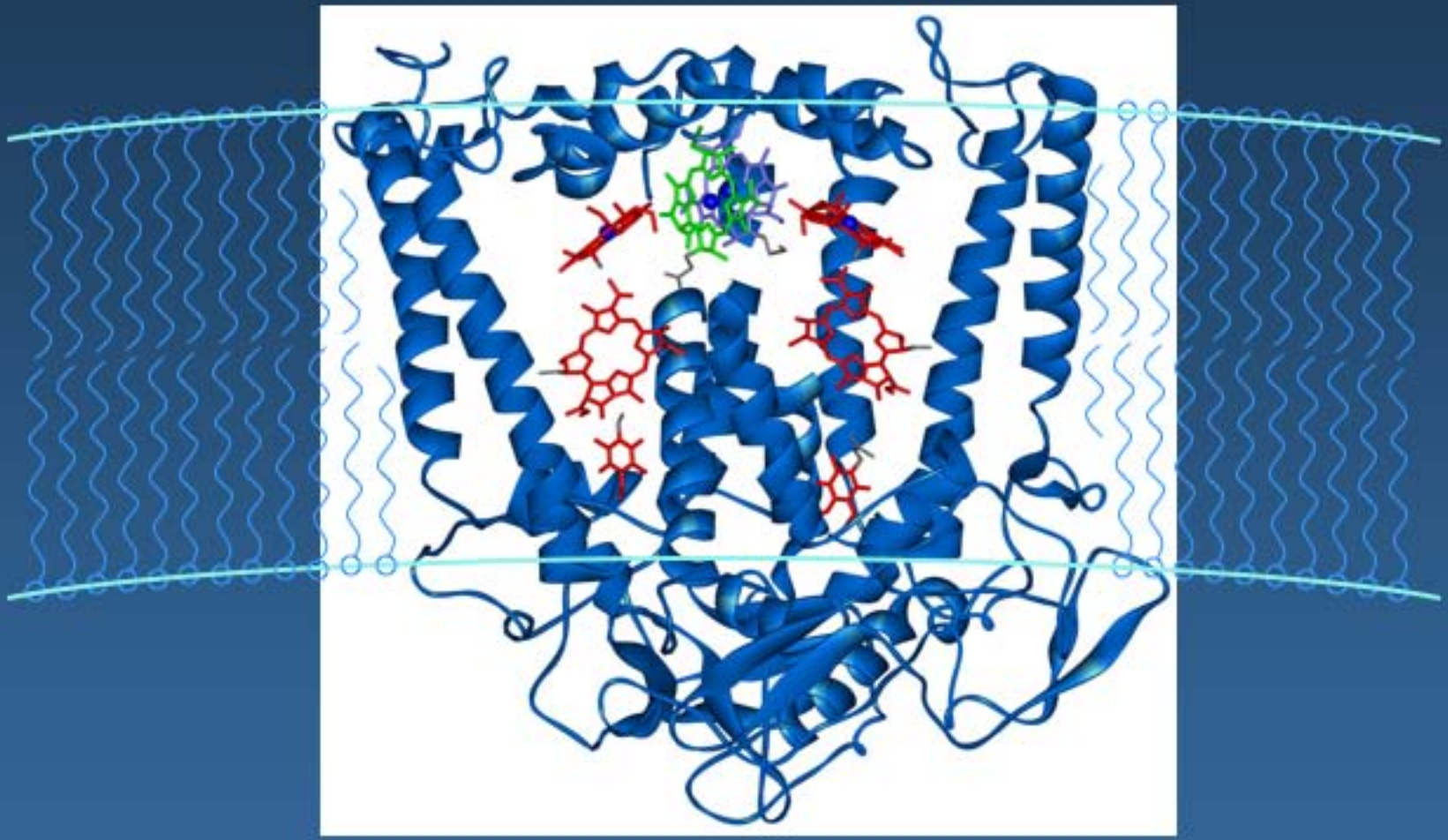

rhodobacter sphaeroides

Stowell, M.H.B.; Rees, D.C.; *et. al. Science* **1997**, *276*, 882.

BChl bacteriochlorophyll
BPheo bacteriopheophytin
Q quinone

photons in
1 oxidant & reductant out

1 step distance : 25 Å
calculated time : ~100 ms

4 steps
ET distance : 55 Å
total time : < 1 ns

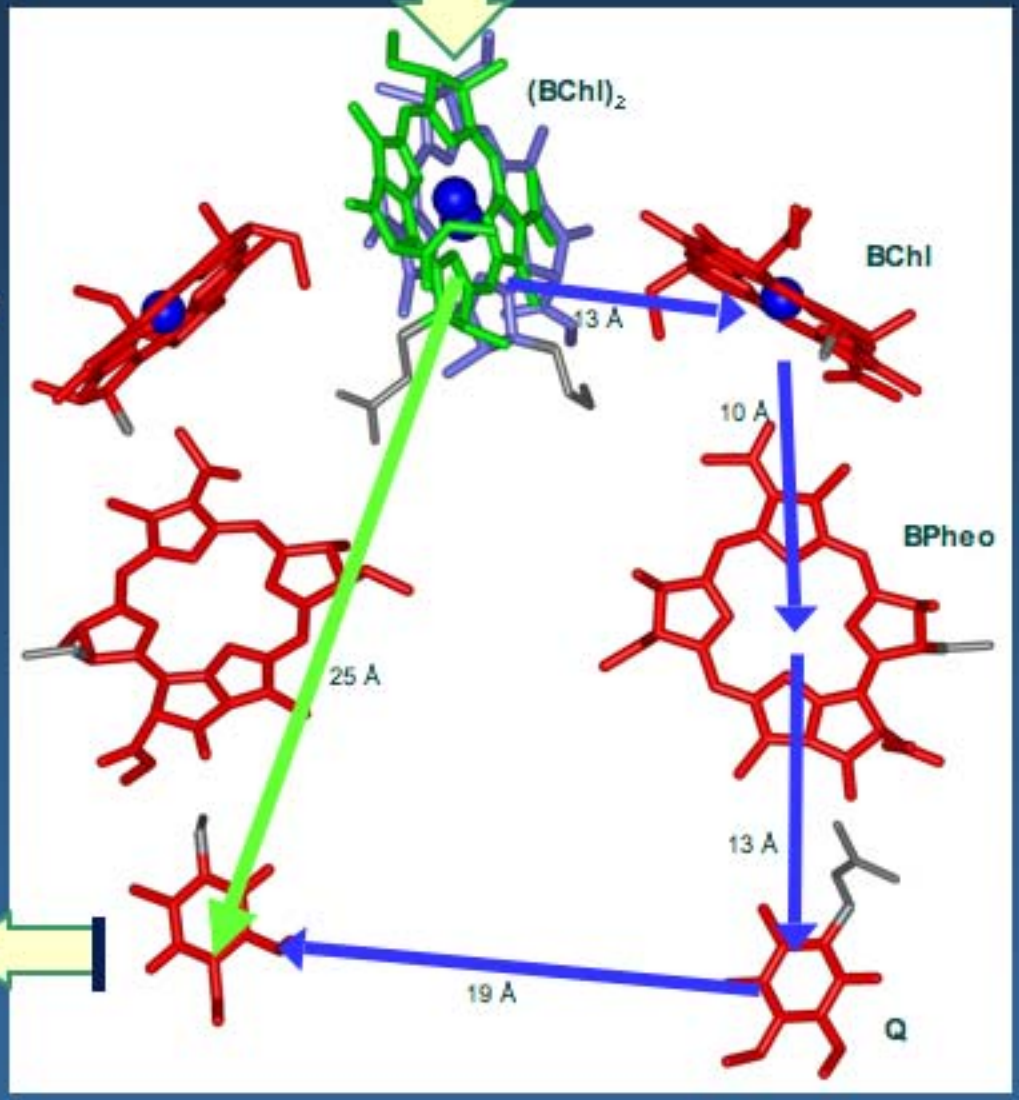

Boxer, S.G. *Annu. Rev. Biophys. Biophys. Chem.* 1990, *19*, 267.

Bacterial Photosynthetic Reaction Center

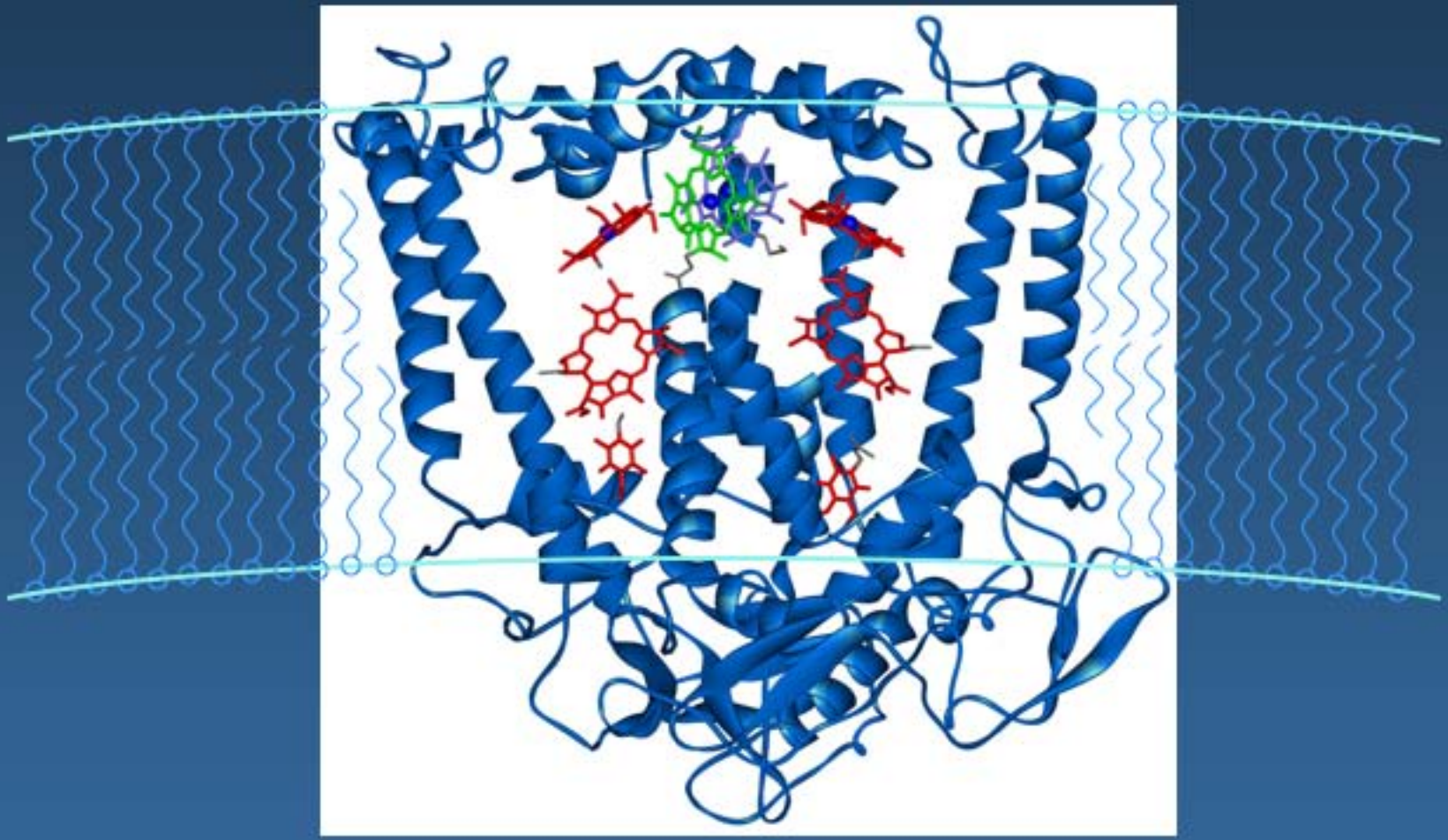

rhodobacter sphaeroides

Stowell, M.H.B.; Rees, D.C.; *et. al. Science* **1997**, *276*, 882.

BChl bacteriochlorophyll
BPheo bacteriopheophytin
Q quinone

photons in
1 oxidant & reductant out

1 step distance : 25 Å
calculated time : ~100 ms

4 steps
ET distance : 55 Å
total time : < 1 ns

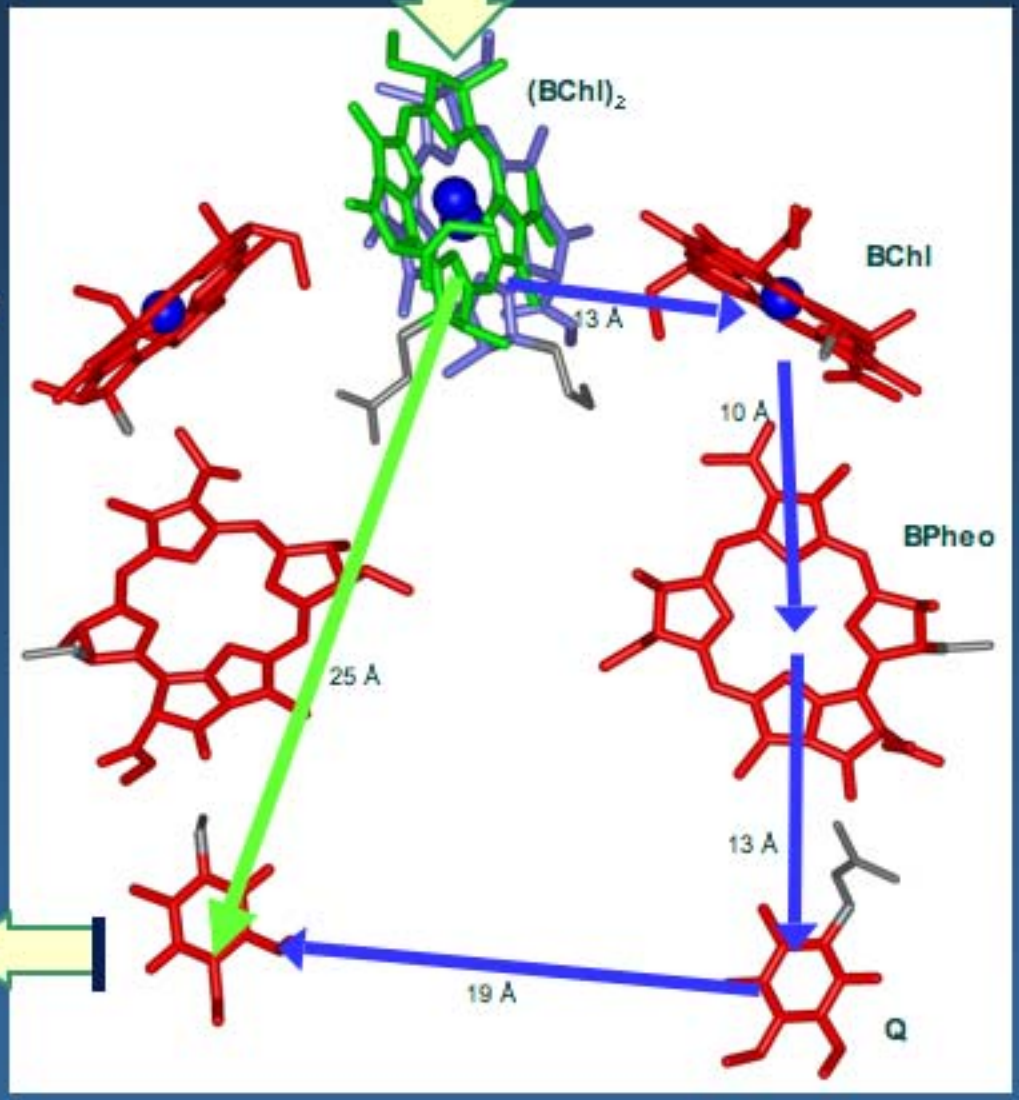

Boxer, S.G. *Annu. Rev. Biophys. Biophys. Chem.* 1990, *19*, 267.

ature uses two photosystems to span the redox space from O_2/H_2O to NAD^+/NAD

Purple Bacteria

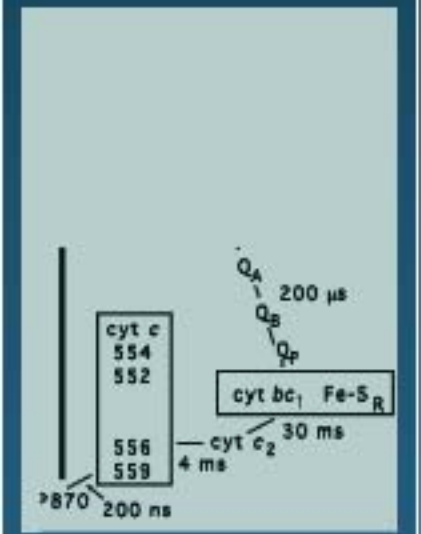

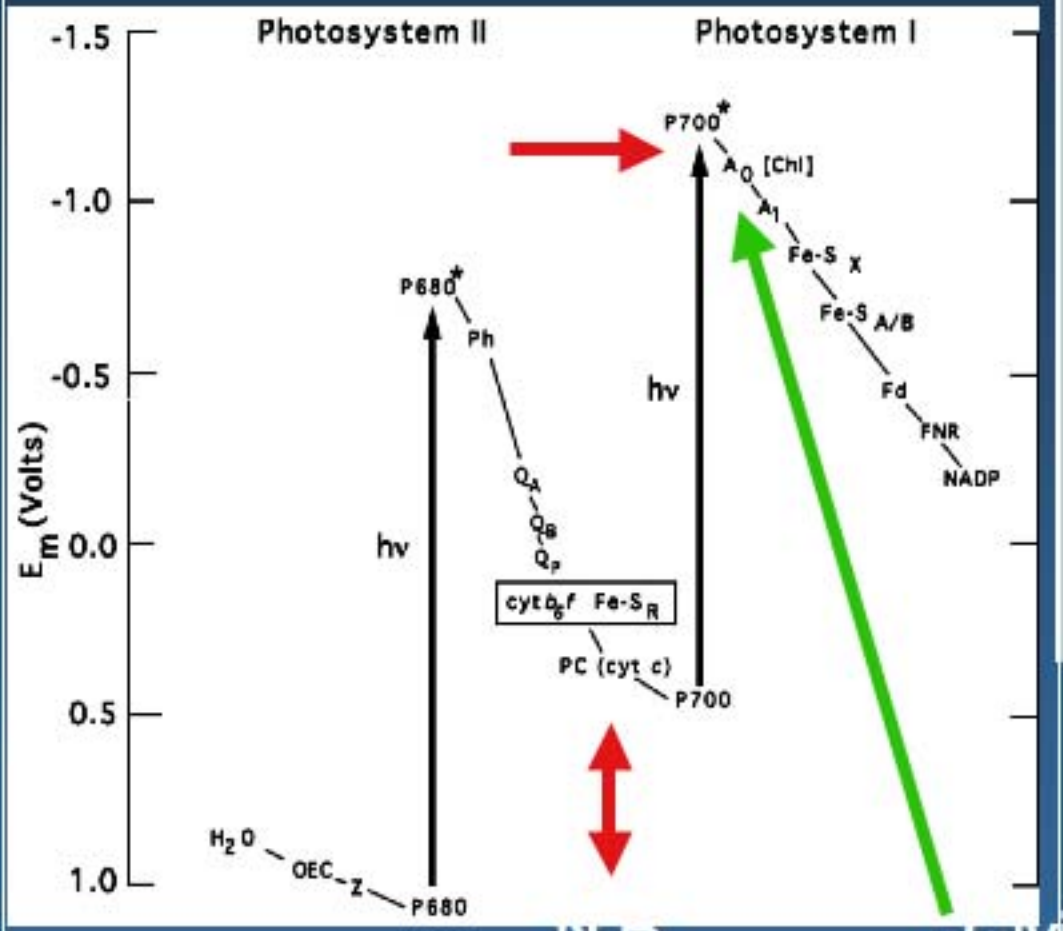

N.B.

Giving more thermodynamic push to synthesis

Thanks to B Blankenship

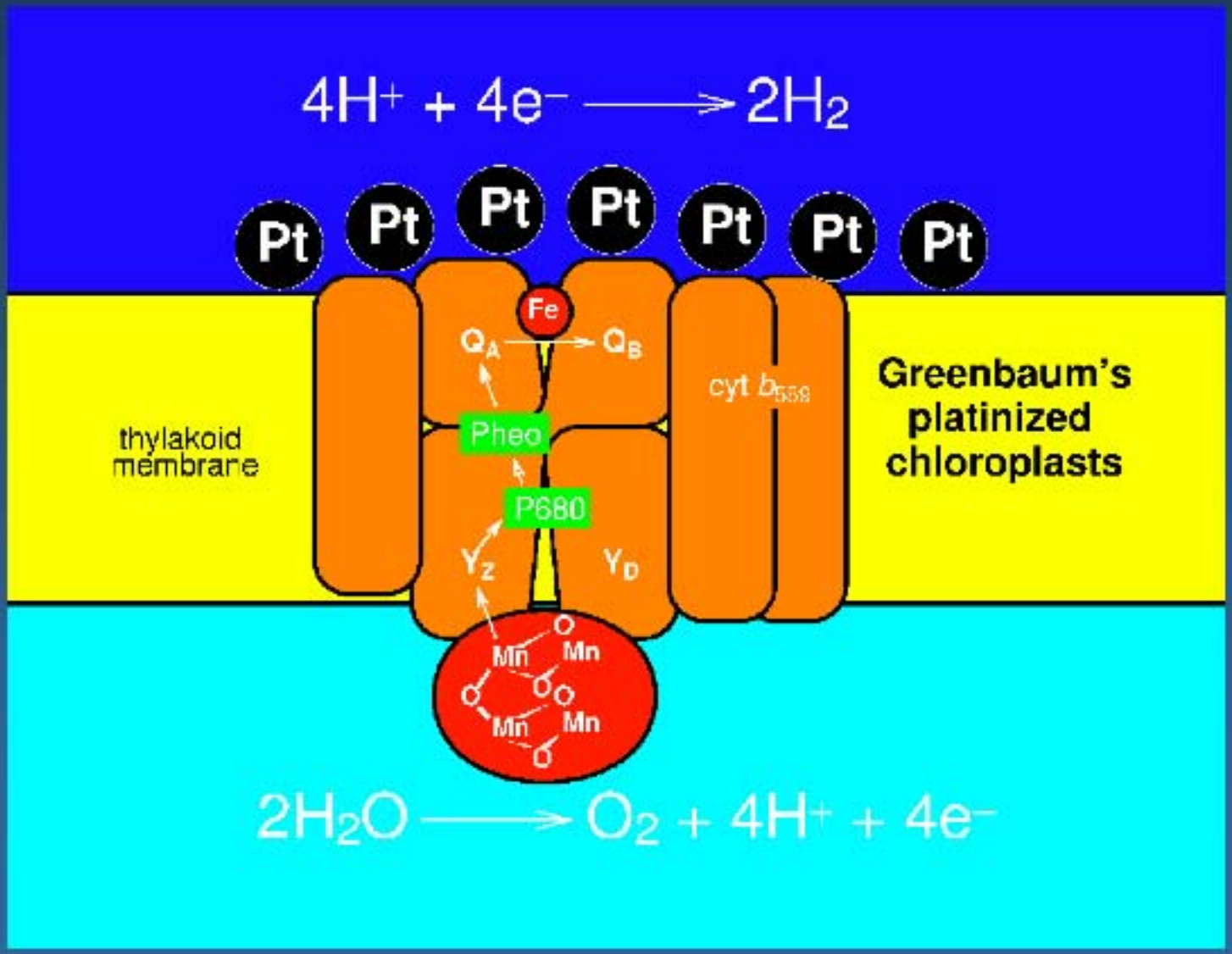
4H+ + 4e− ⟶ 2H2
Pt
Pt
Pt
Pt
Pt
Pt
Pt
Fe
QA
QB
cyt b559
Pheo
P680
YZ
YD
thylakoid membrane
Greenbaum's platinized chloroplasts
Mn
Mn
Mn
Mn
O
2H2O ⟶ O2 + 4H+ + 4e−

Energy Conversion Strategies

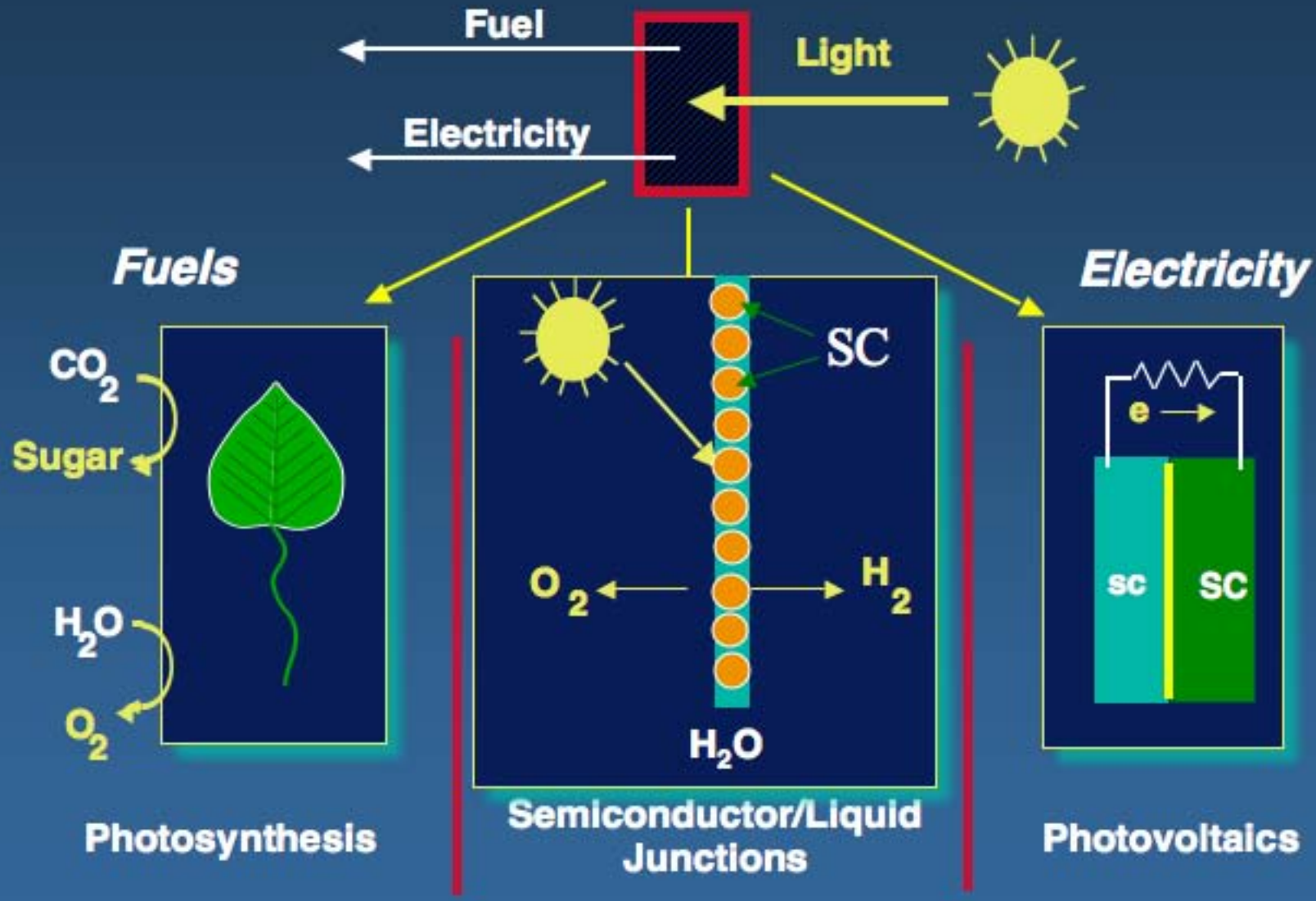

Photovoltaic + Electrolyzer System

Photoelectrolysis System

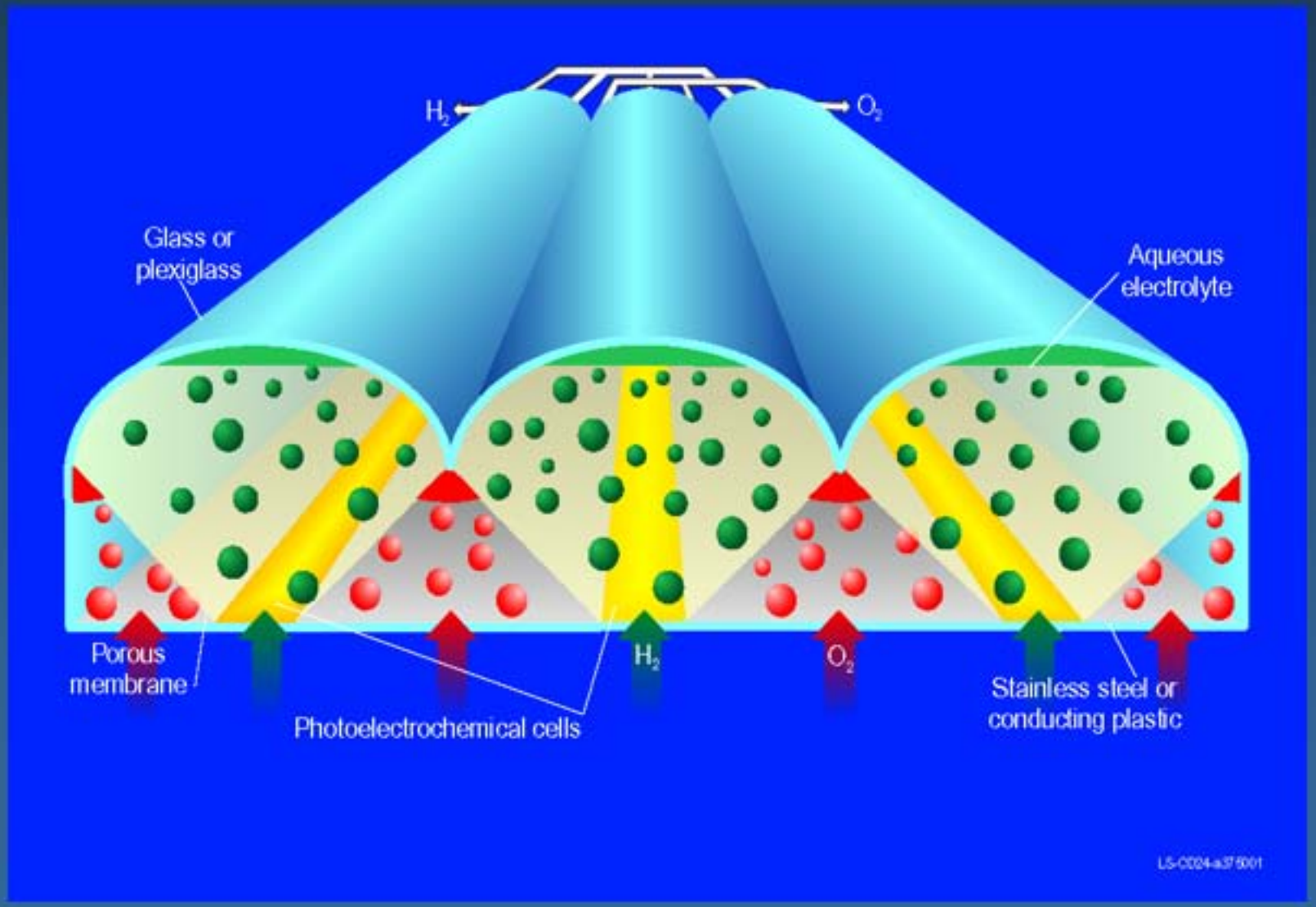

Energy Conversion Strategies

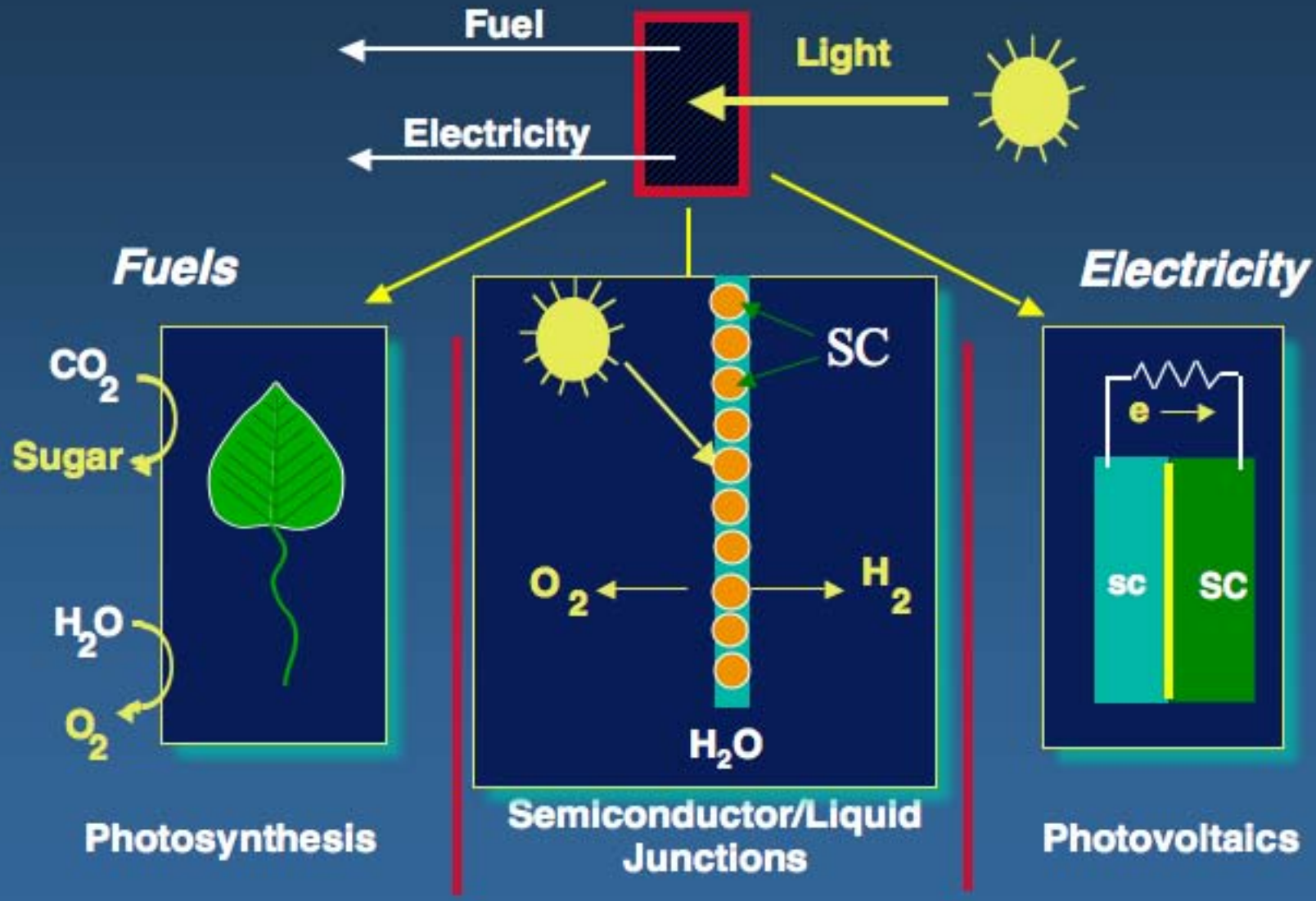

Fuel from Sunlight

Photoelectrochemical Cell

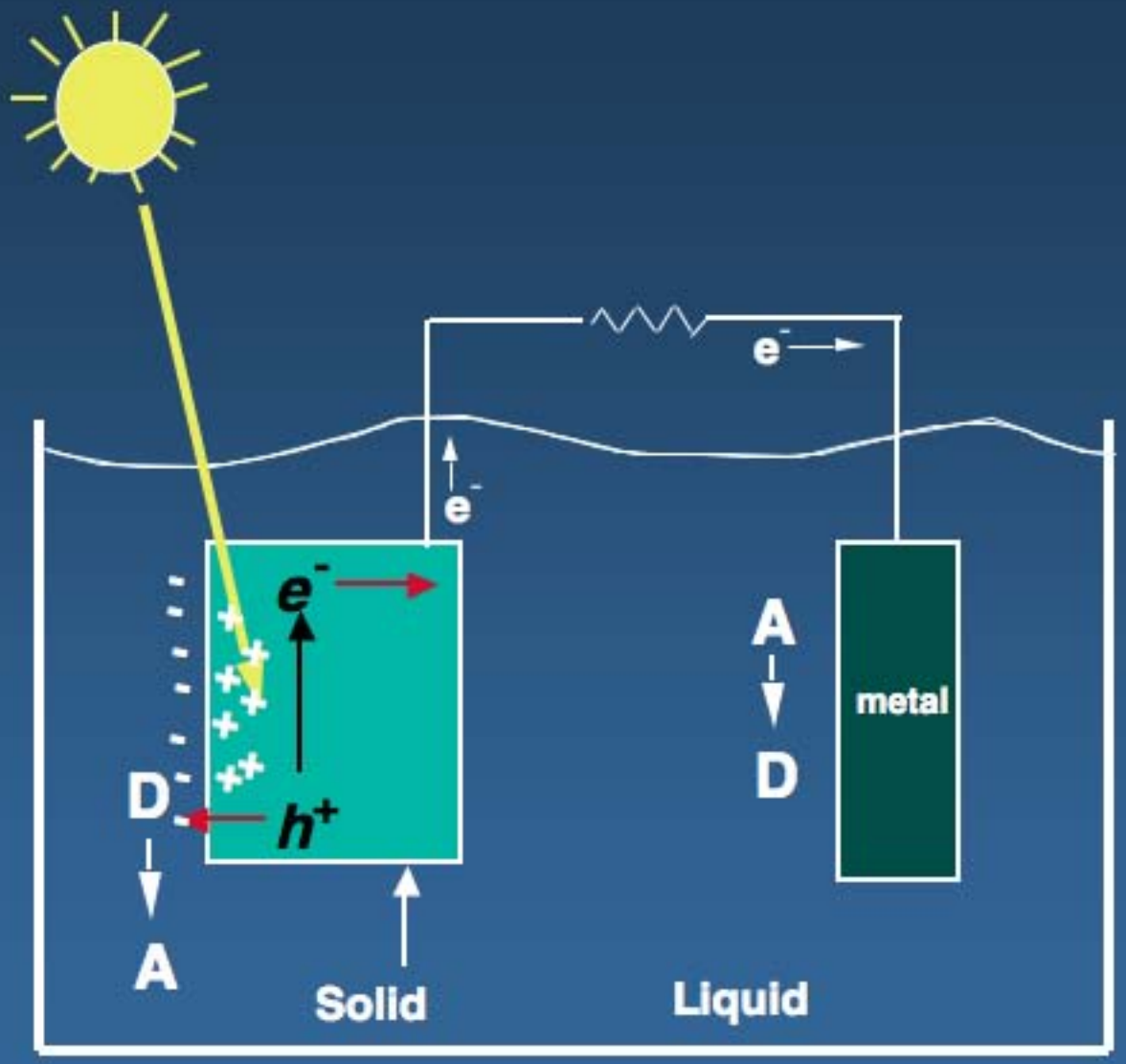

Light is Converted to Electrical+Chemical Energy

Photoelectrochemical Cell

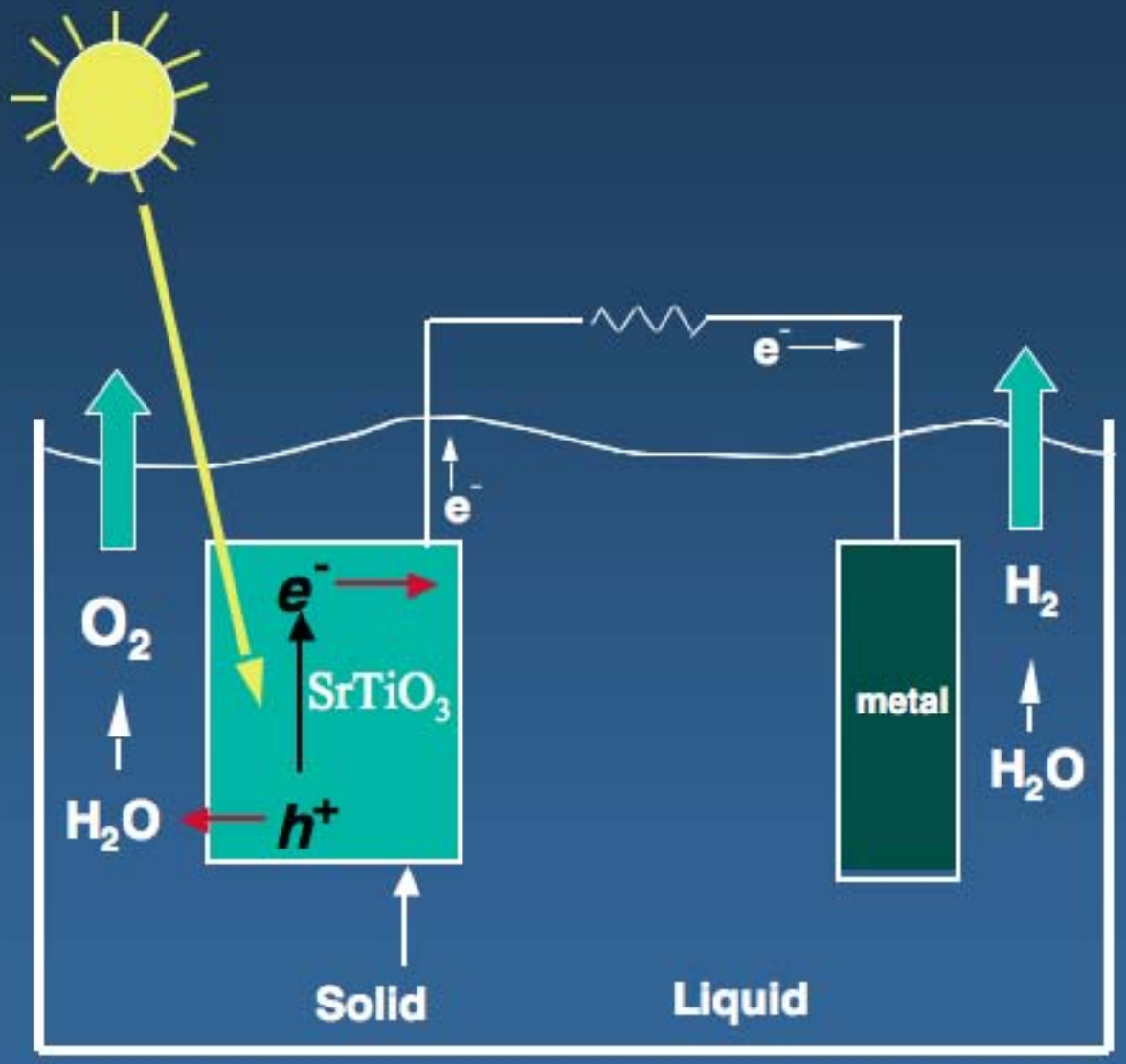

Light is Converted to Electrical+Chemical Energy

Photoelectrochemical Cell

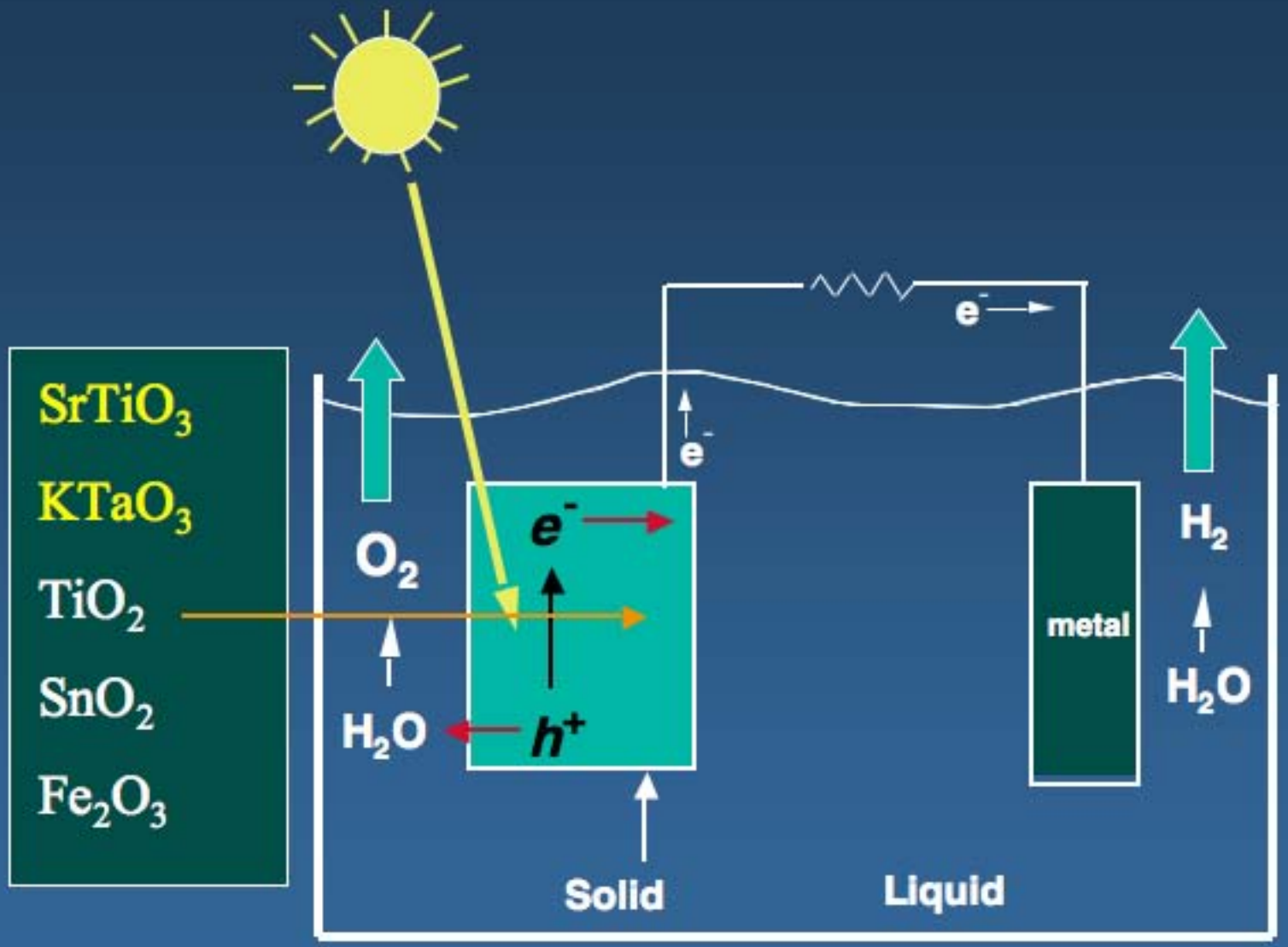

Light is Converted to Electrical+Chemical Energy

Optimum Absorption Threshold

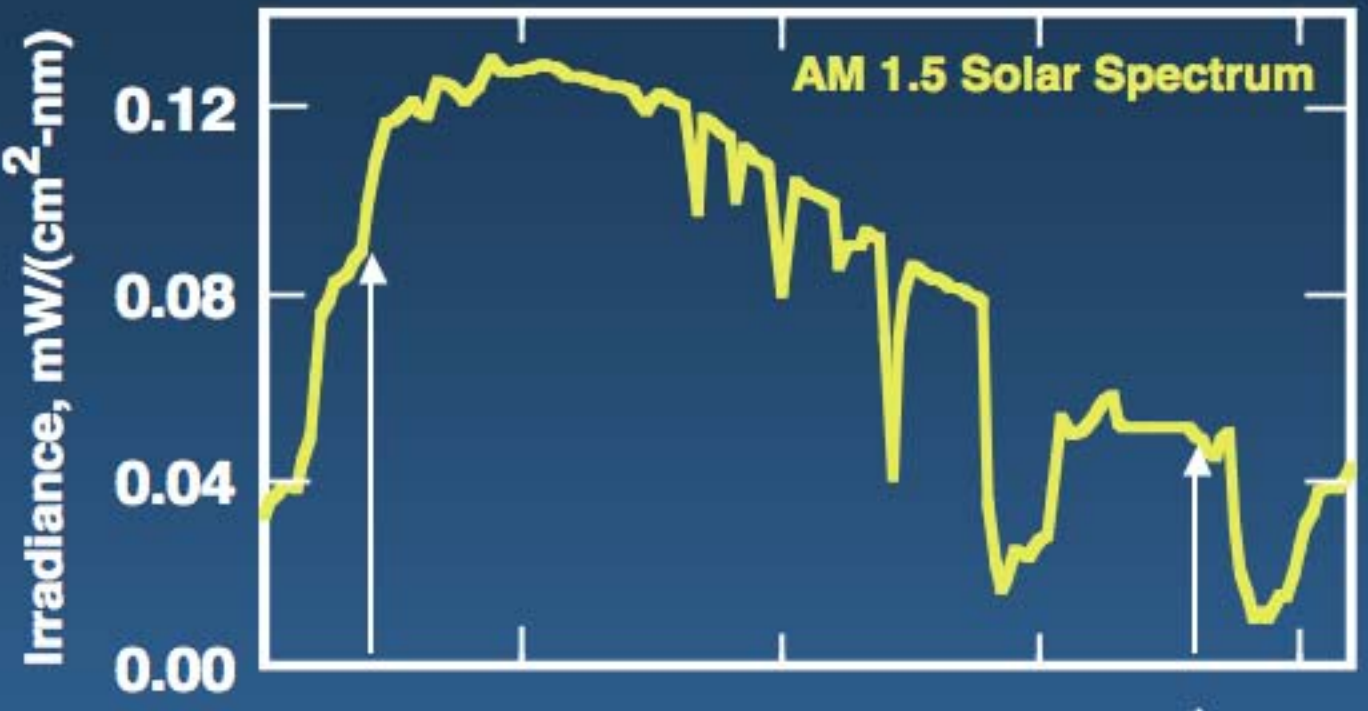

Too Large
Band Gap

Too Small
Band Gap

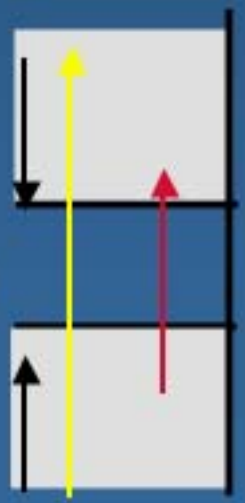

Solar H_2 production on $Ru/CuInS_2$-$AgInS_2$-ZnS solid solution photocatalyst

Solar simulator(AM-1.5)

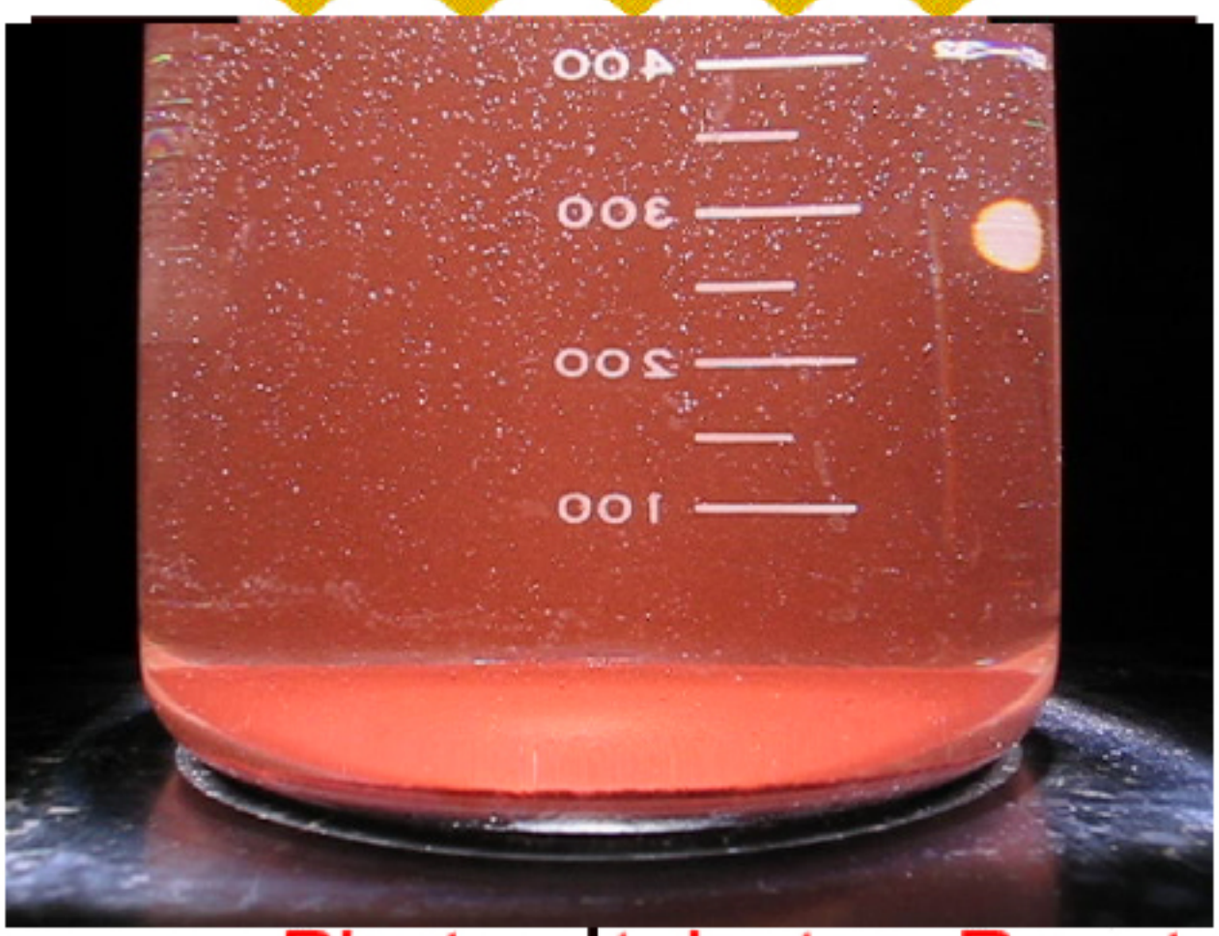

Rate of H_2 evolution
8L/h•m²

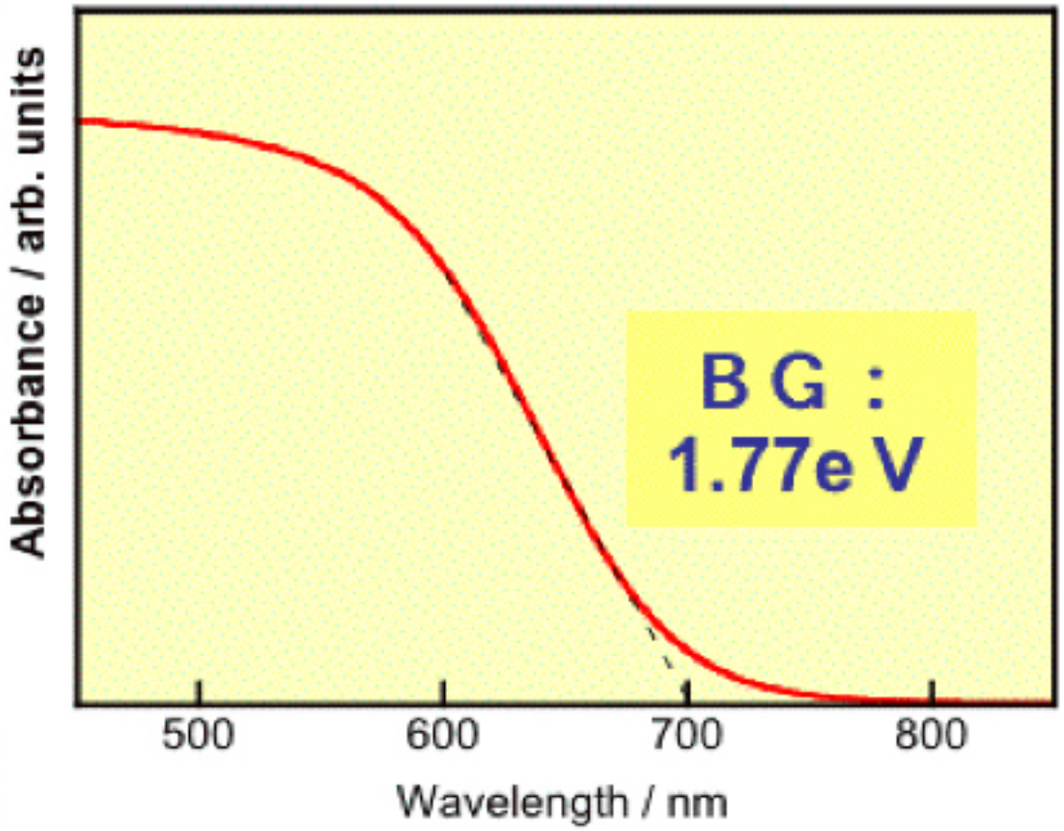

Photocatalyst Reactant: K_2SO_3 + Na_2S

I. Tsuji, H. Kato, and A. Kudo,
Angew. Chem., Int. Ed., 44, 3565 (2005), *Chem. Mater., 18, 1969* (2006).

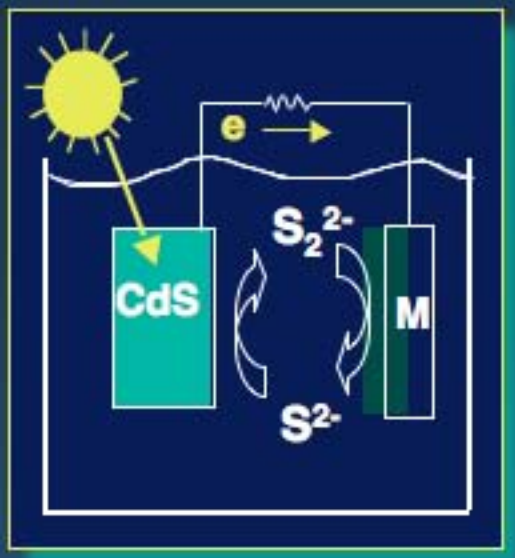

New Redox Couples

Nonaqueous Solvents

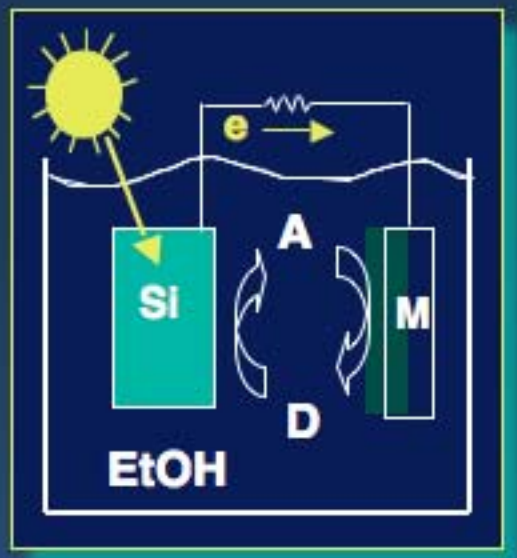

Four Strategies

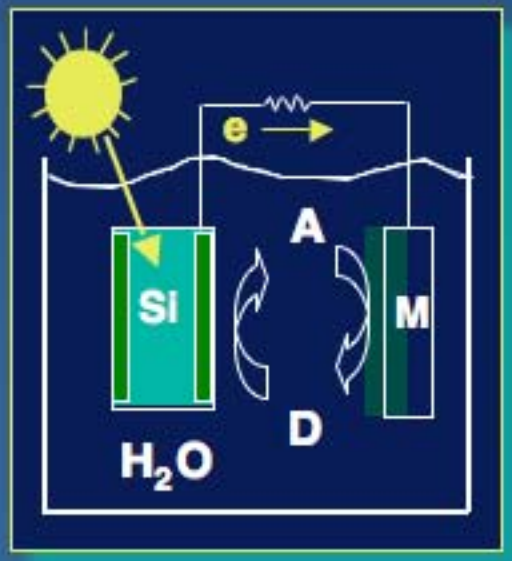

Surface Modification

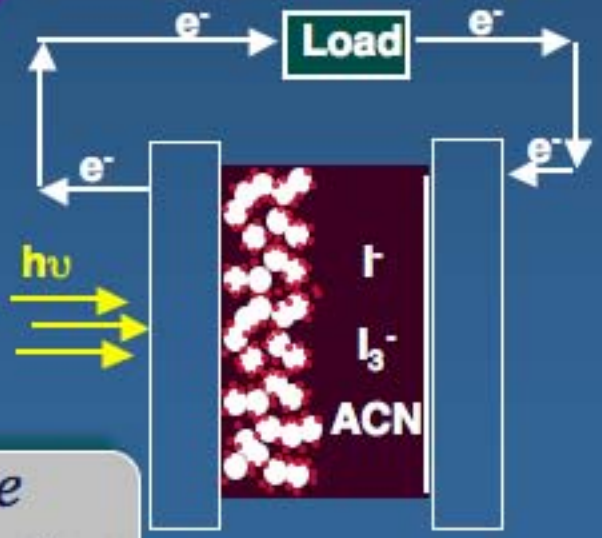

Inexpensive Semiconductors

Combinatorial Discovery of Nanorod Materials

FTO slide printed with binary combinations of eight metals, pyrolyzed to form mixed metal oxides.

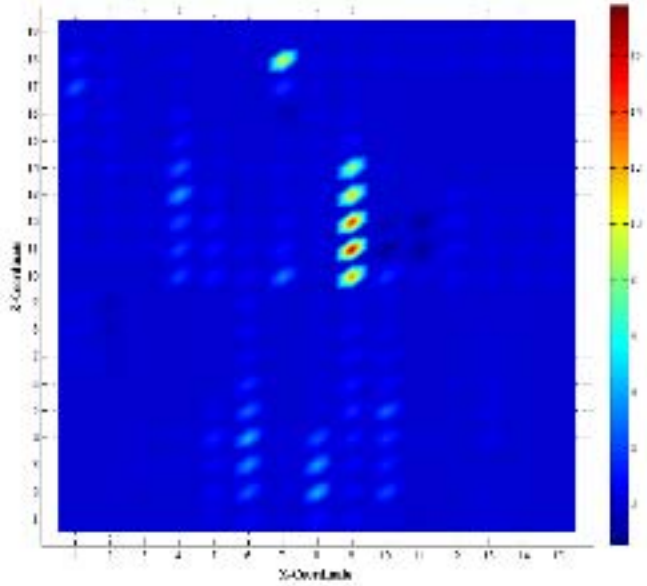

Typical photocurrent map of a slide of metal oxides. The X- and Z-coordinates give each spot's identity, which is correlated with photo-catalytic activity. Here, combinations of Zn and Co in row #9 show photoanodic current

Fuel Cell vs Photoelectrolysis Cell

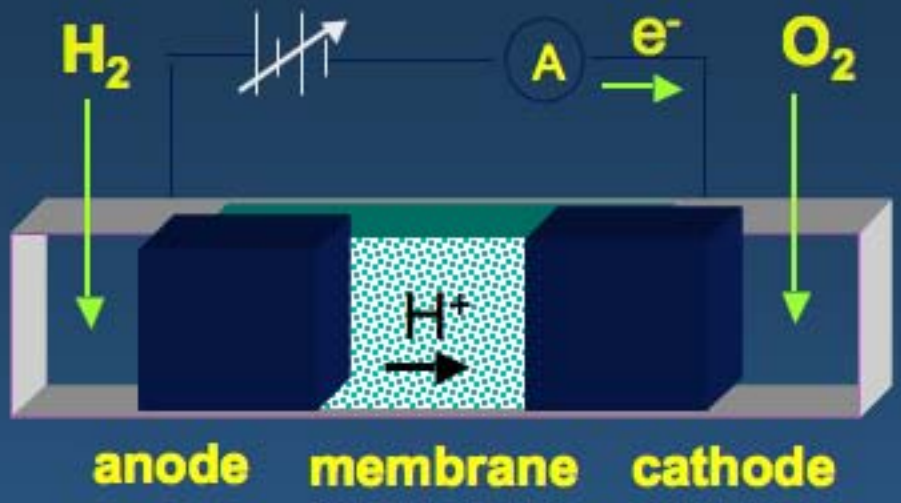

Fuel Cell MEA

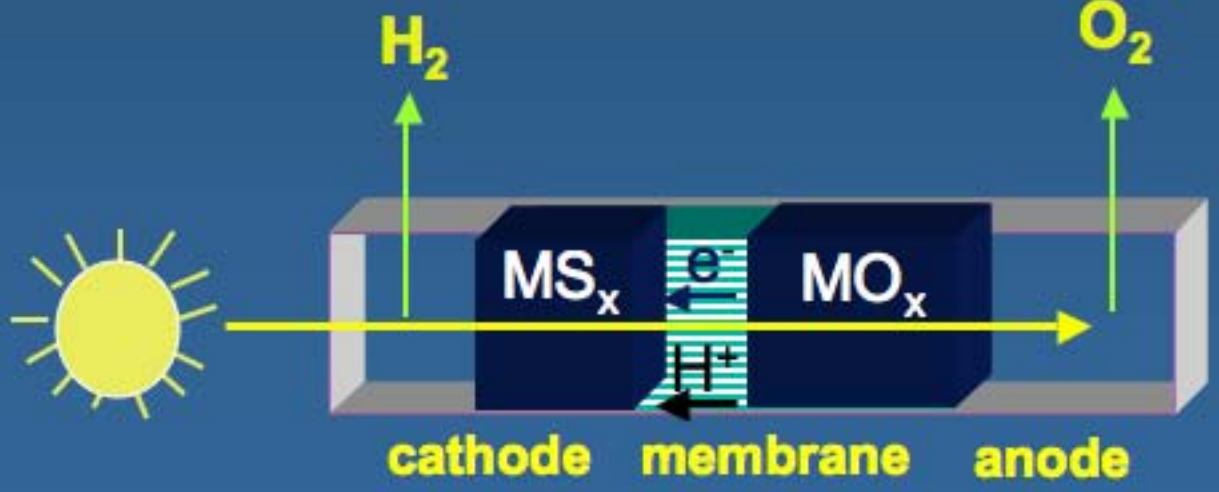

Photoelectrolysis Cell MEA

Towards a Solar Fuels System

M. Calvin, 1982: It is time to build an actual artificial photosynthetic system, to learn what works and what doesn't work, and thereby set the stage for making it work better

2007 Goal: To demonstrate a manufacturably scalable solar fuel generator, using earth-abundant elements, that, with no wires, robustly produces fuel from the sun, 10 times more efficiently than (current) crops

Lessons from Photosynthesis

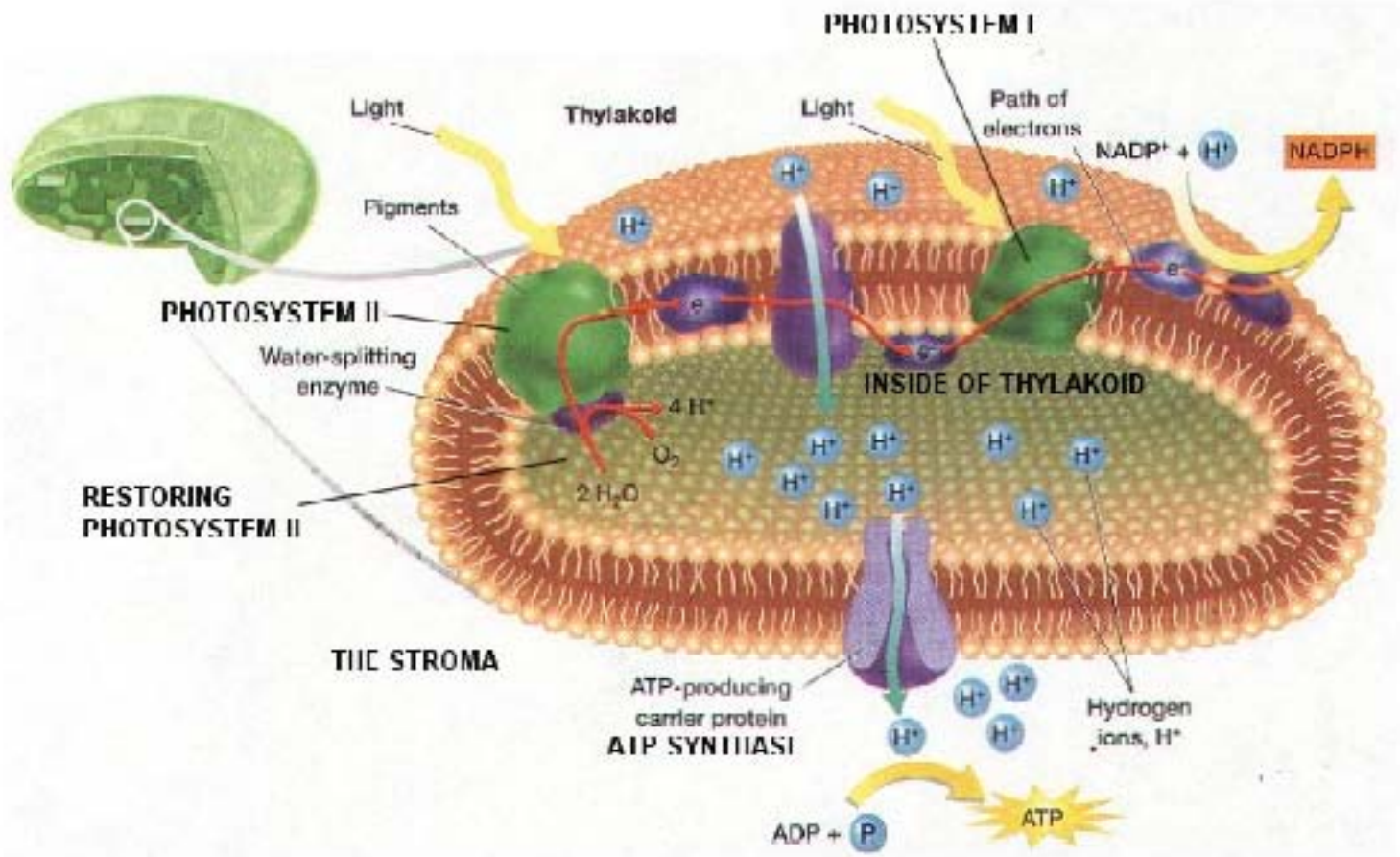

System Concept

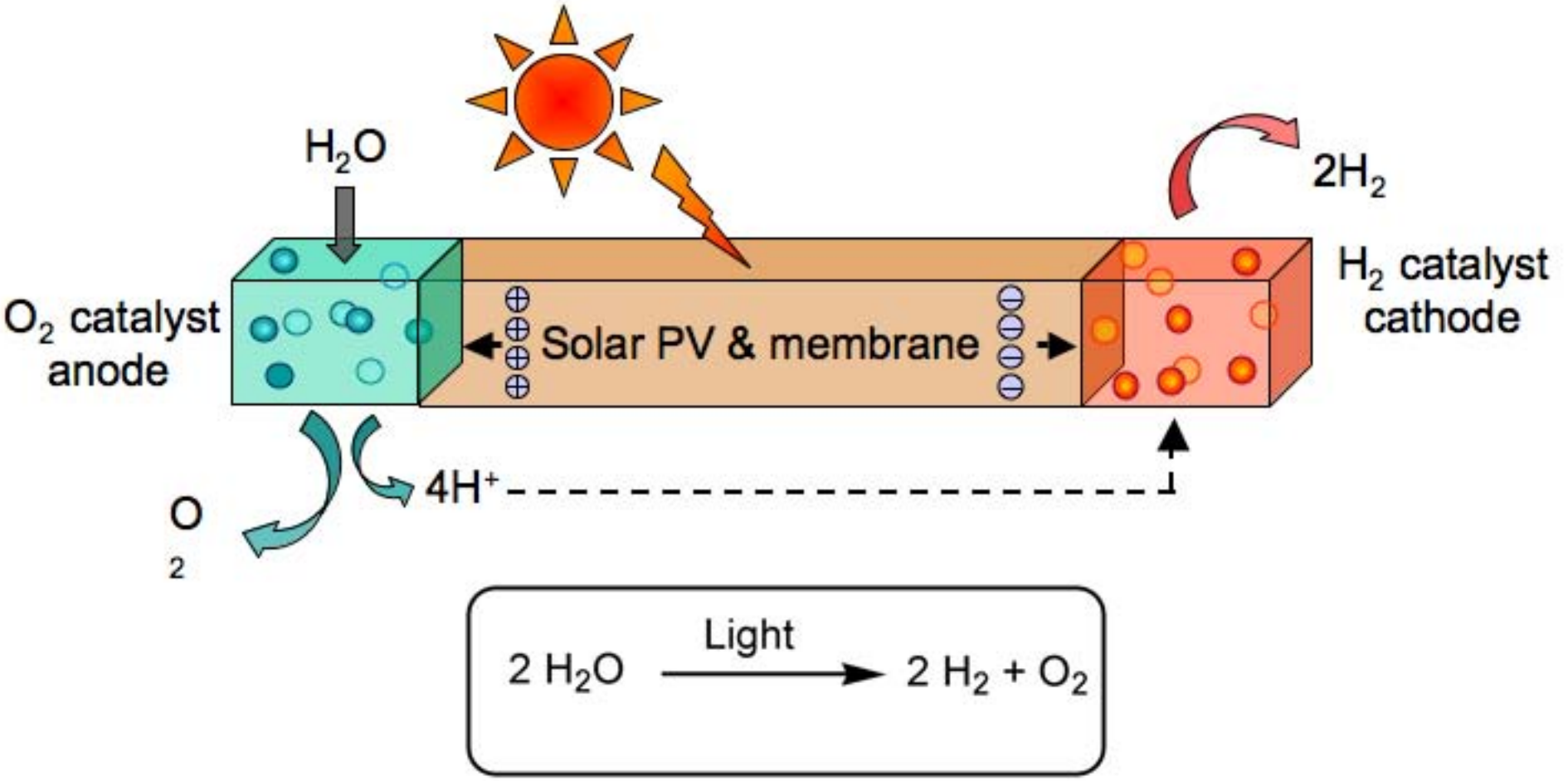

Turner Cell

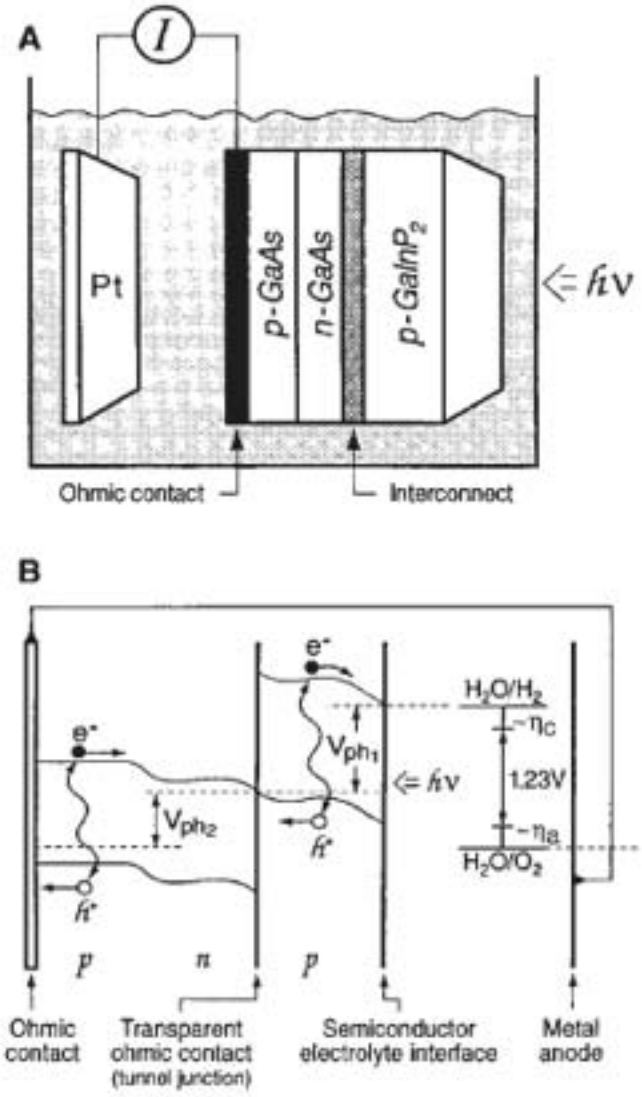
A
I
Pt
p-GaAs
n-GaAs
p-GaInP2
⇐ hν
Ohmic contact
Interconnect
B
e⁻
e⁻
Vph1
Vph2
⇐ hν
h⁺
h⁺
H2O/H2
-ηc
1.23V
-ηa
H2O/O2
p
n
p
Ohmic contact
Transparent ohmic contact (tunnel junction)
Semiconductor electrolyte interface
Metal anode

Why Radial Junction Solar Cells?

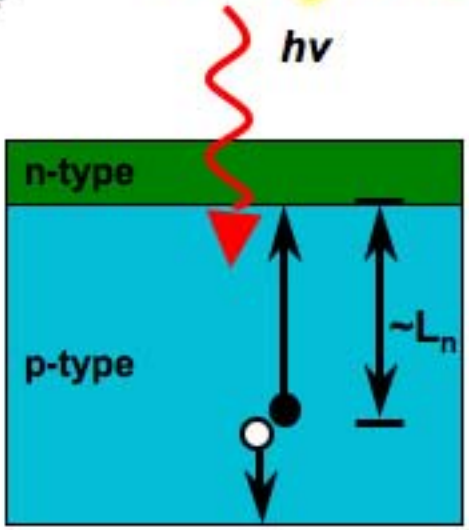

Traditional single junction solar cell

- Traditional device design requires long minority carrier diffusion lengths, and therefore expensive materials

Why Radial Junction Solar Cells?

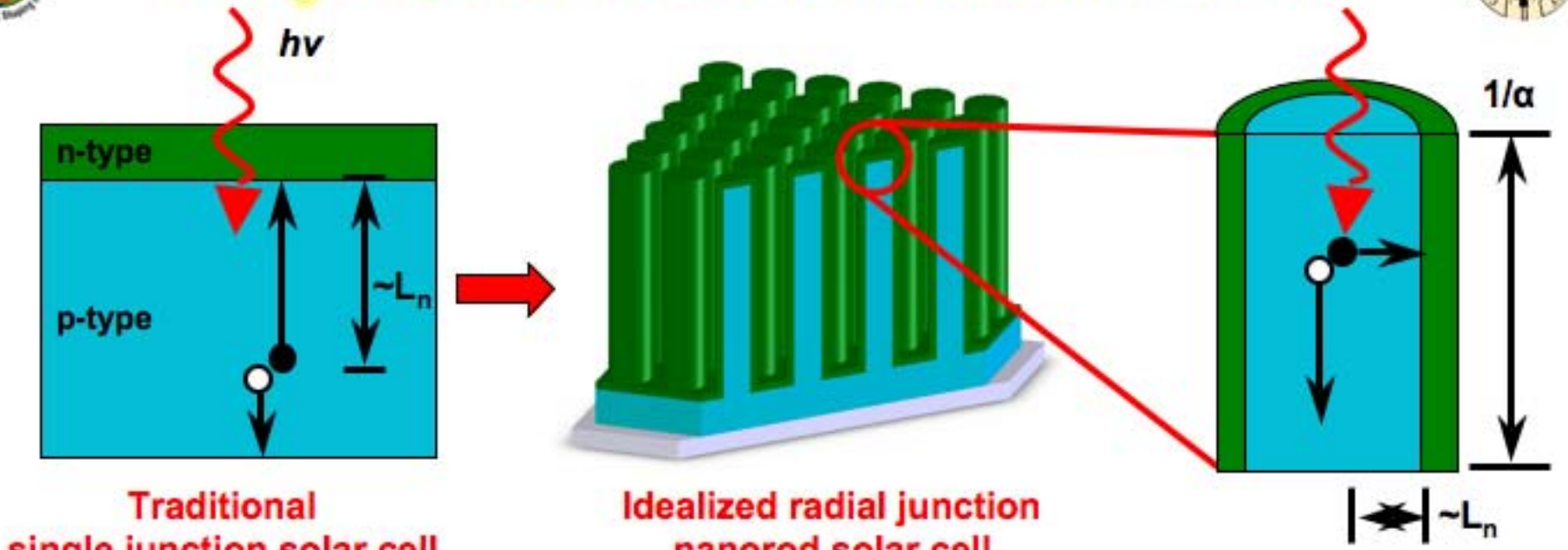

- Traditional device design requires long minority carrier diffusion lengths, and therefore expensive materials

- **Radial geometry allows for high quantum efficiency despite short minority carrier diffusion lengths**

Device Modeling

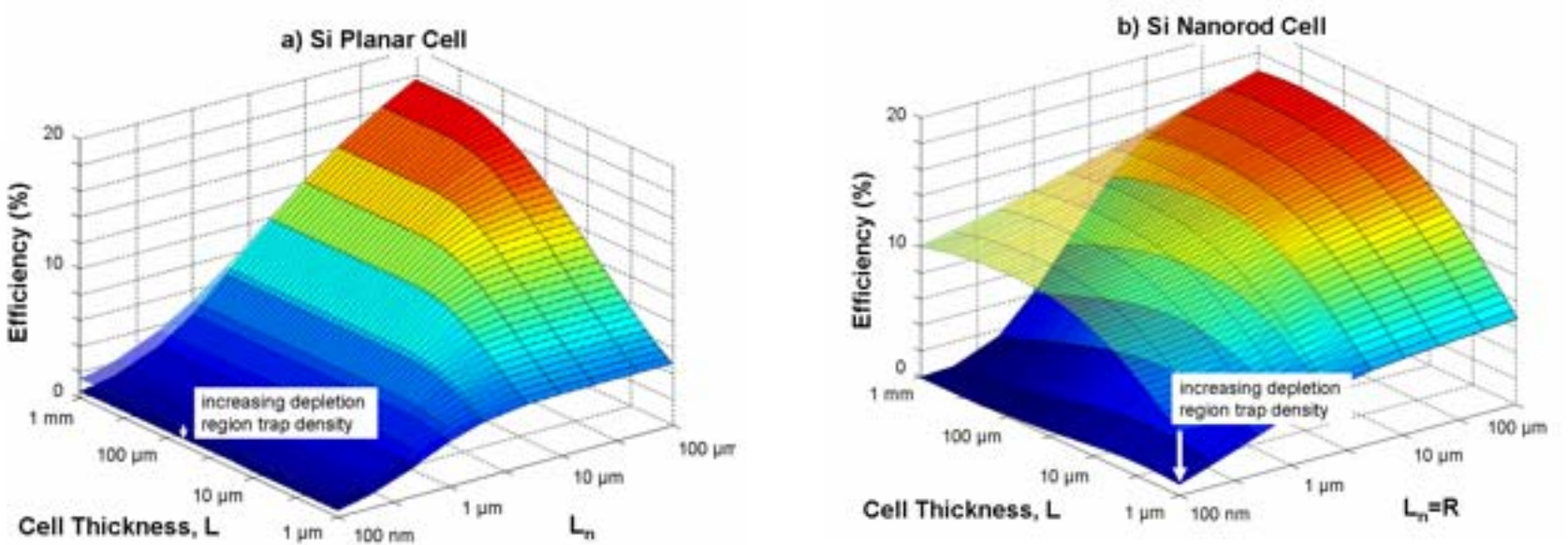

Comparison of photovoltaic efficiency for (a) planar and (b) nanowire Si devices as a function of absorber thickness and minority carrier diffusion length

Relatively high efficiencies possible despite low diffusion lengths if depletion region recombination can be minimized

B.M. Kayes, H. A. Atwater, and N. S. Lewis, *J. Appl. Phys.* 97 114302 (2005)

Structural Organization in Nature

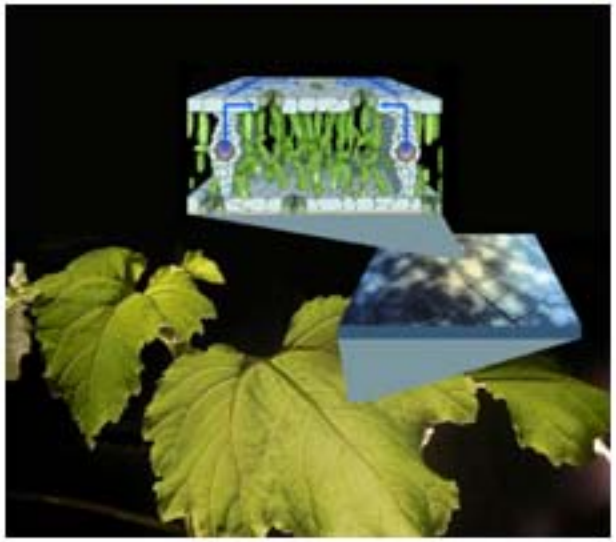

Stomata

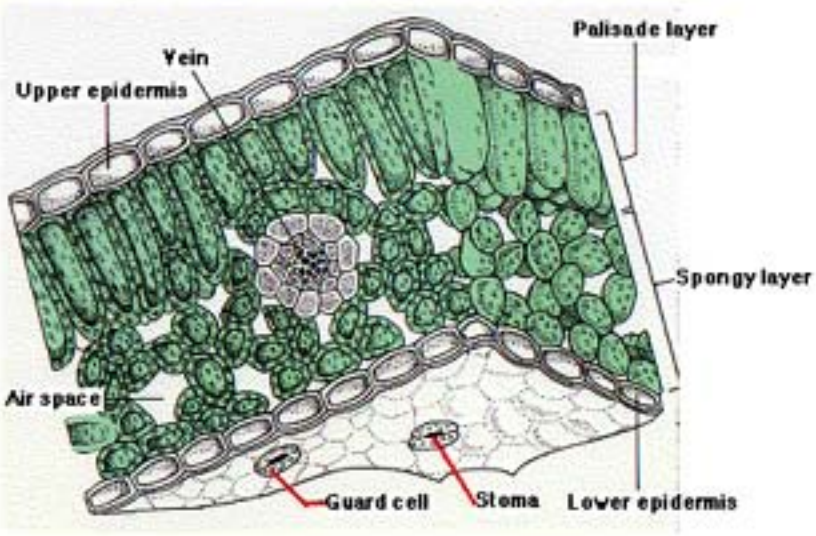

Leaf

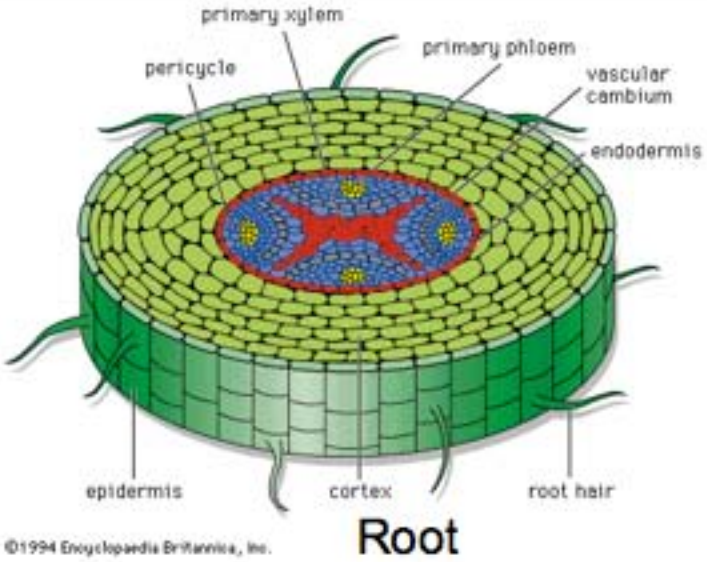

Root

Forest

Enables New Materials

- High efficiencies possible despite low diffusion lengths

=> Inexpensive materials

- **Cheaper traditional materials**
  - Silicon as a model system
- **Non-traditional, earth-abundant materials**
  - Tandem partners with silicon

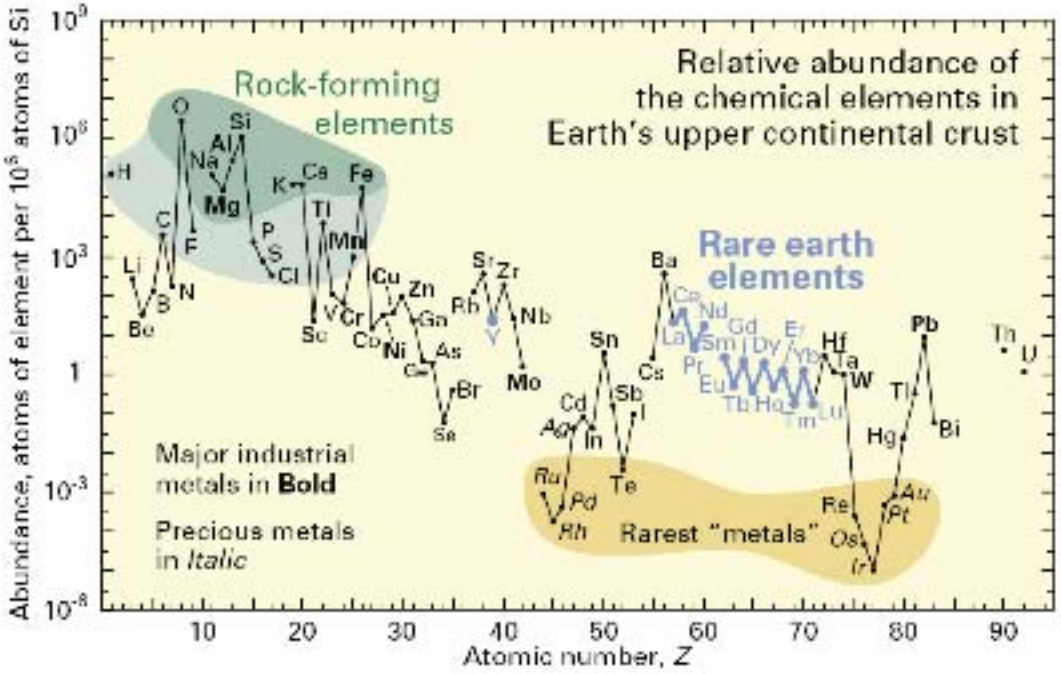

Hydrogen Evolution Reaction

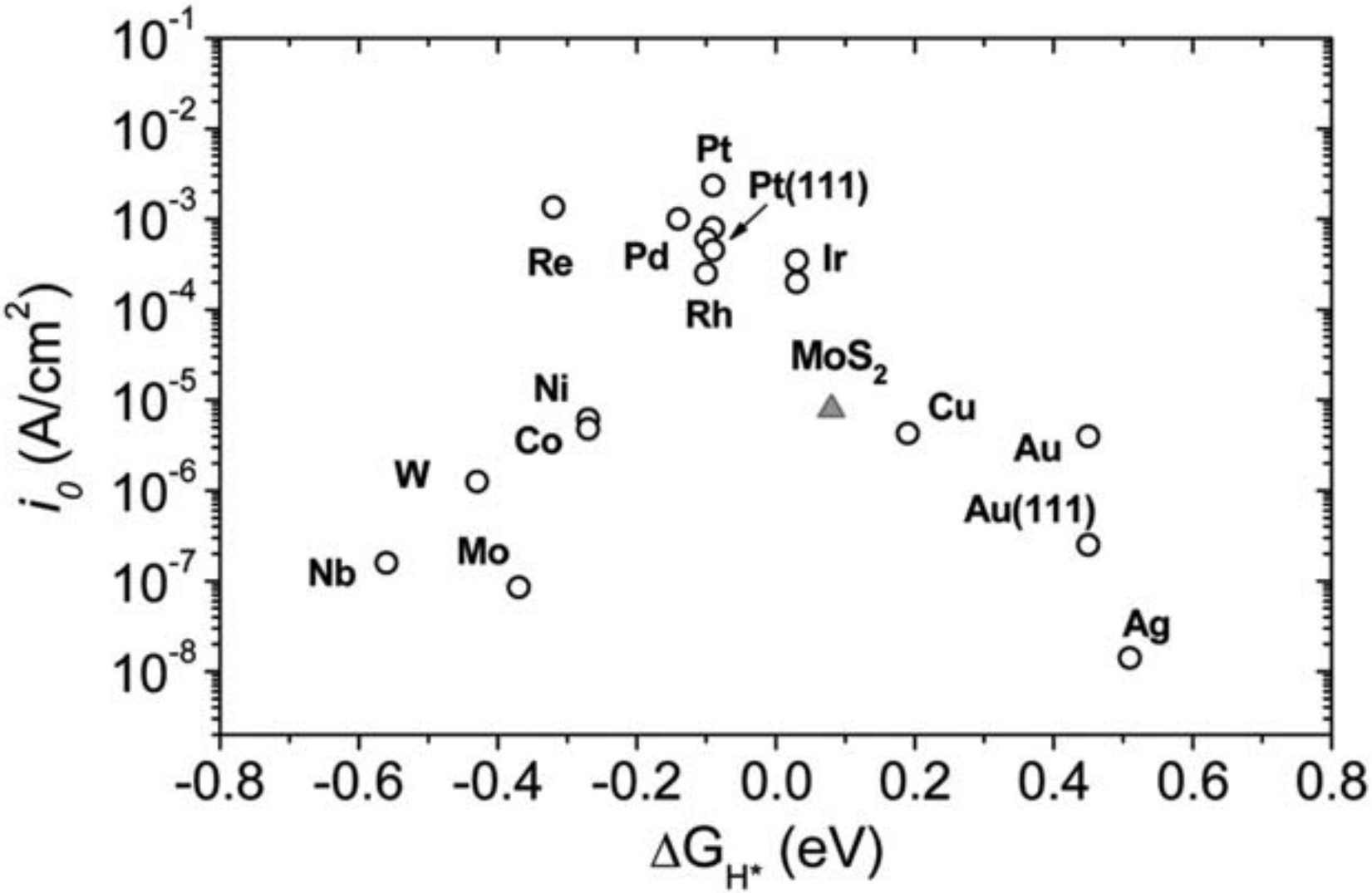

The Alumina Template

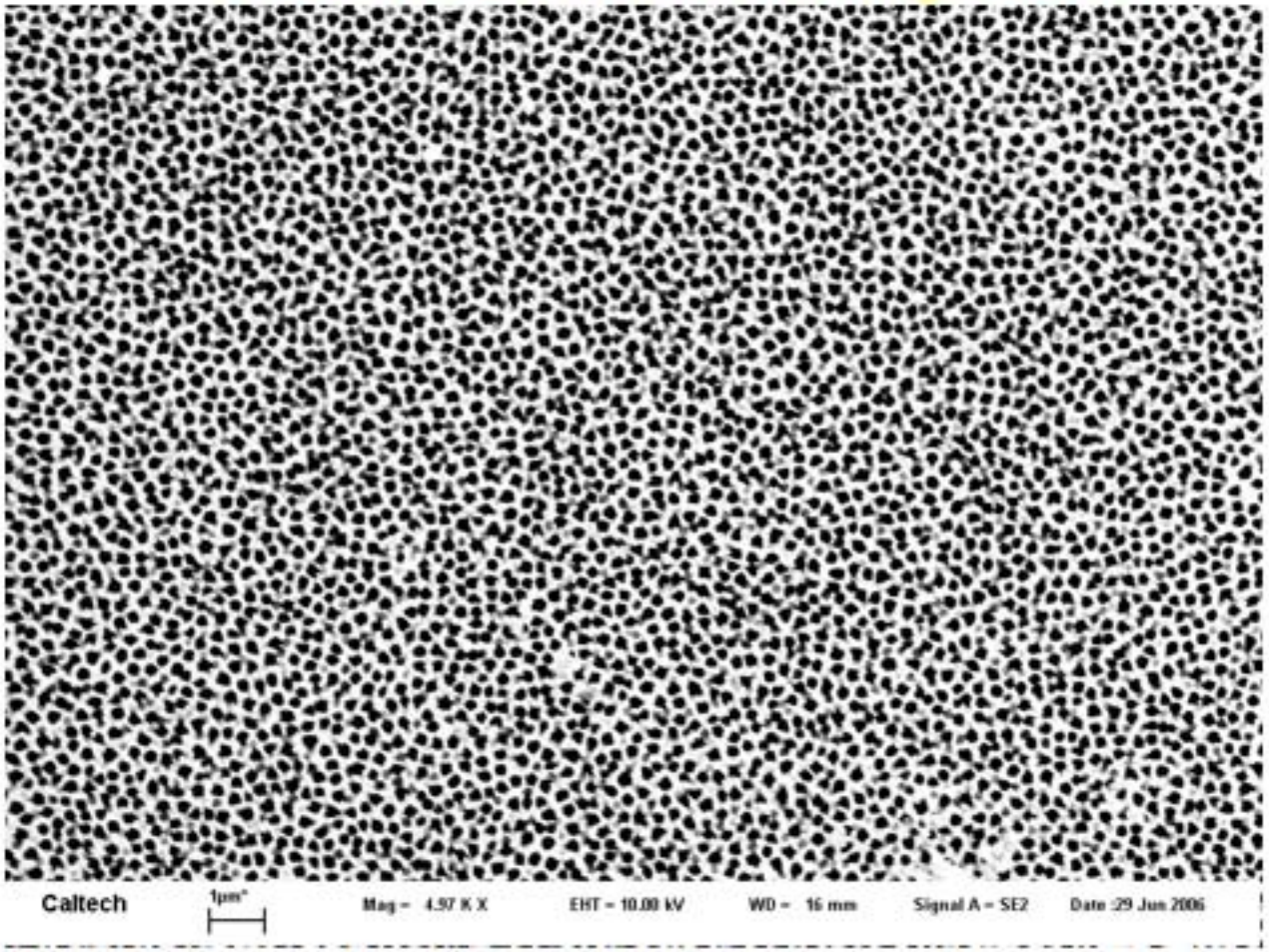

- Allows for dense, uniform array of rods
- Carefully controlled dimensions
- Easily removable template

The Alumina Template

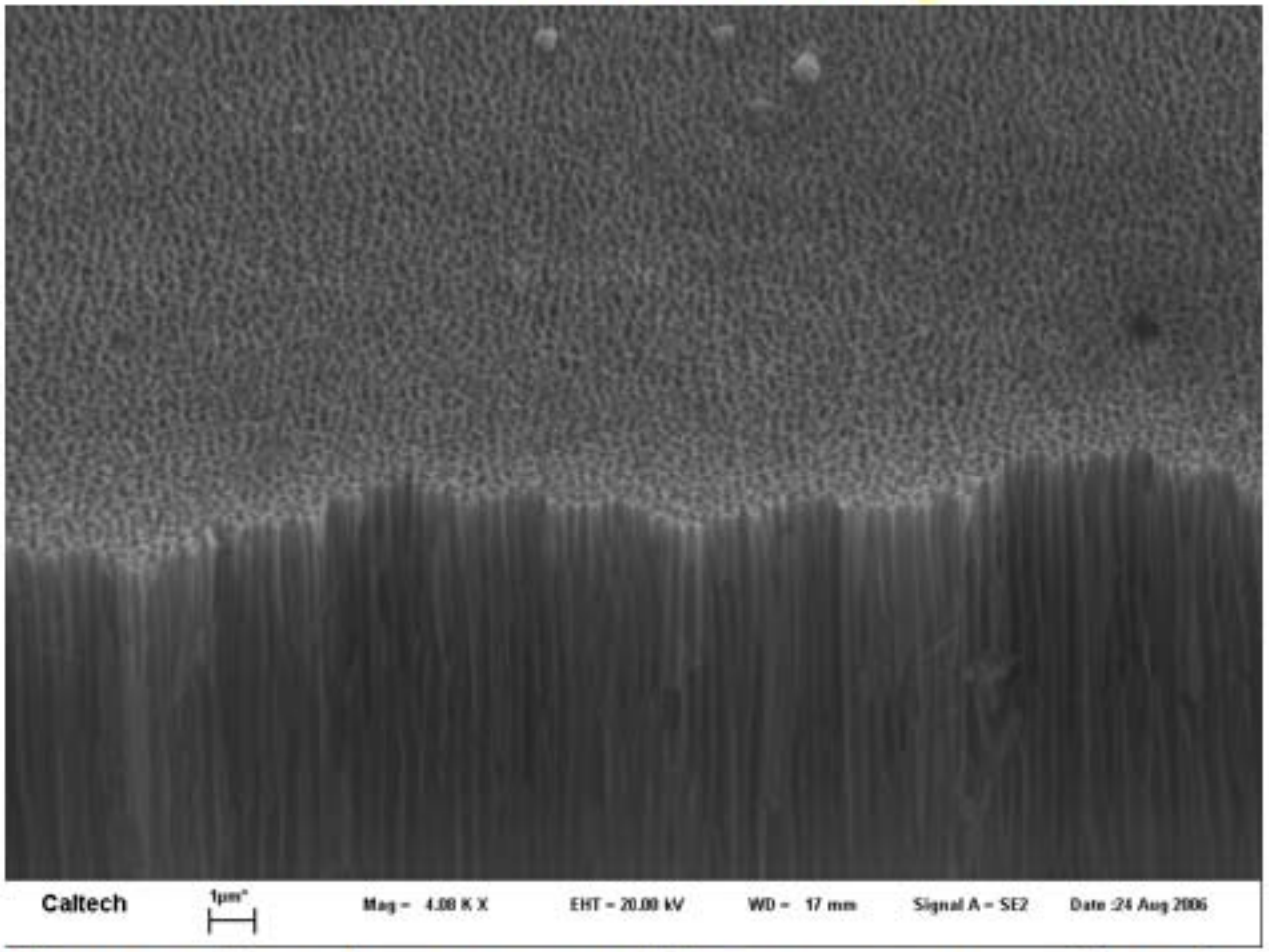

- Allows for dense, uniform array of rods
- Carefully controlled dimensions
- Easily removable template

CdSeTe Nanorods

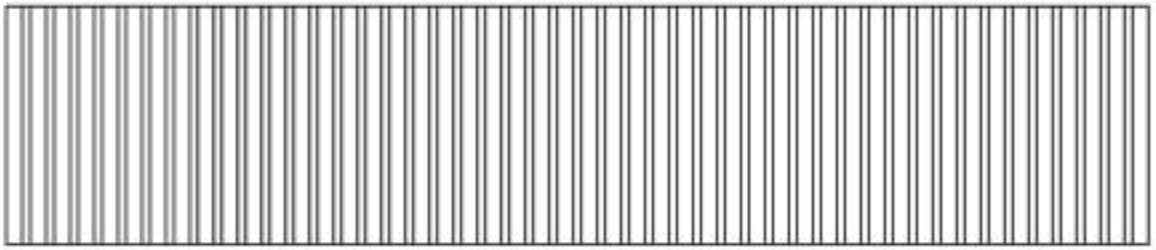

Porous Alumina

CdSeTe Nanorods

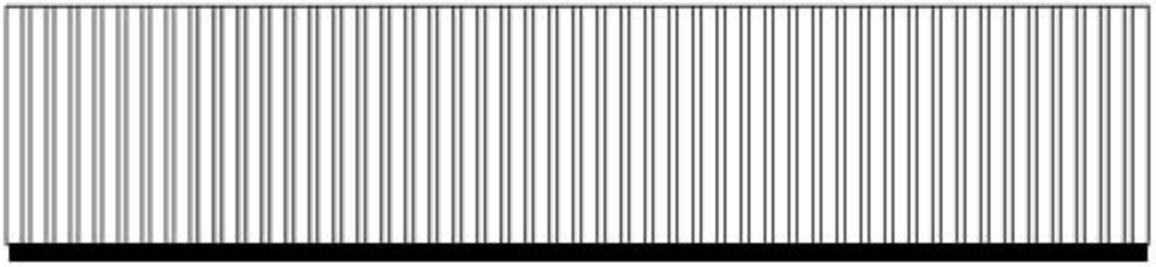

Porous Alumina

CdSe layer to prevent shunting (via sputtering)

CdSeTe Nanorods

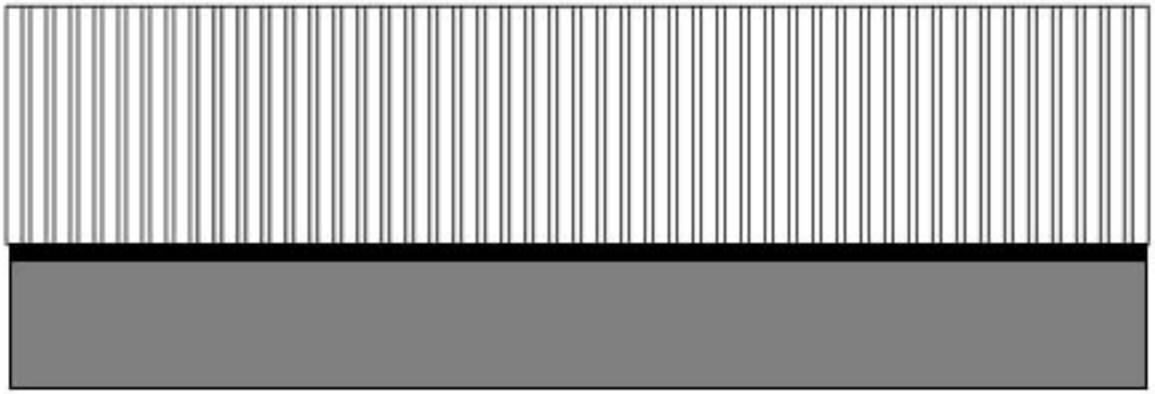

Porous Alumina

CdSe layer to prevent shunting (via sputtering)

Titanium Back Contact (via sputtering)

CdSeTe Nanorods

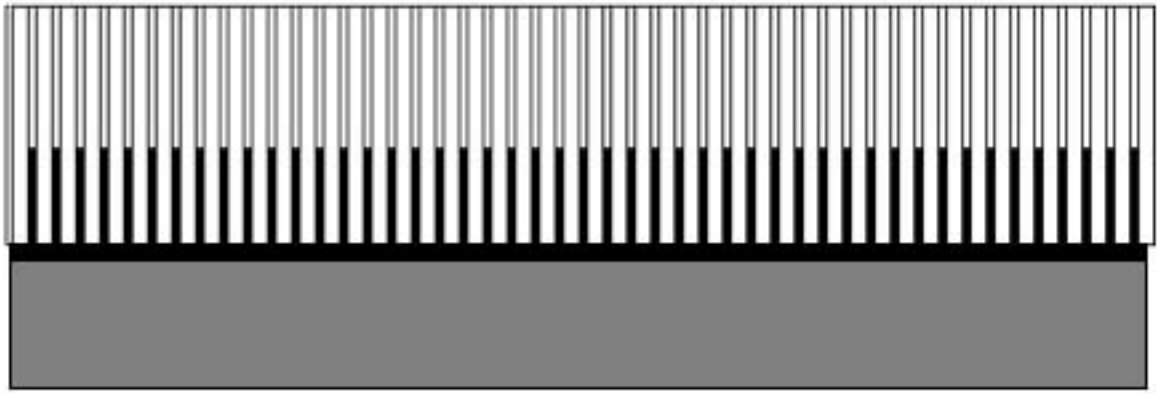

Porous Alumina

CdSeTe Nanorods (via electrodeposition)

CdSe layer to prevent shunting (via sputtering)

Titanium Back Contact (via sputtering)

CdSeTe Nanorods

Alumina template removed in 1 M NaOH

Porous Alumina

CdSeTe Nanorods (via electrodeposition)

CdSe layer to prevent shunting (via sputtering)

Titanium Back Contact (via sputtering)

CdSeTe Nanorods

- Use a liquid junction to make a photoelectrochemical cell
- Measure current-voltage properties in the dark and light and compare nanorod performance to an analogous planar electrode

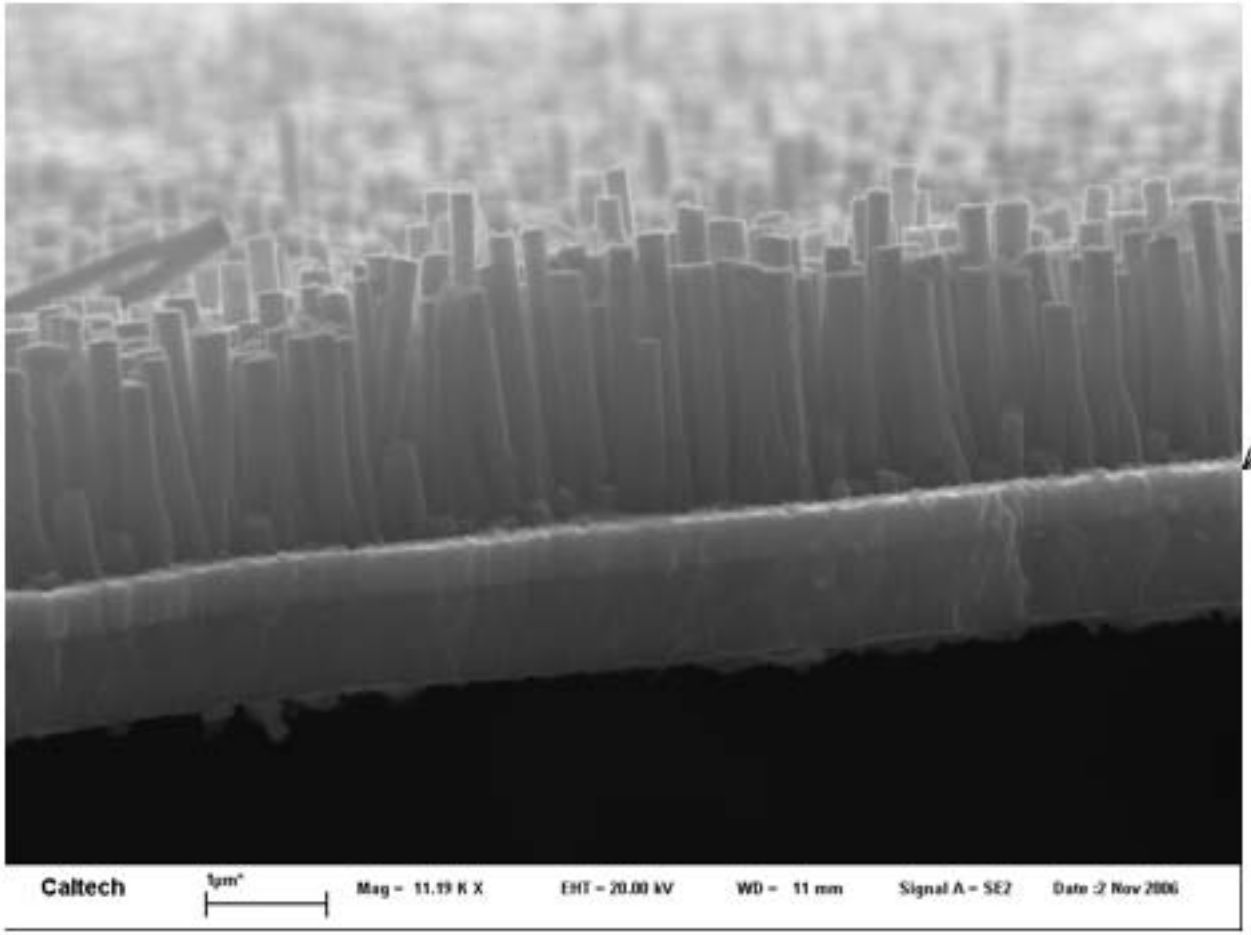

- Thin sputtered CdSe layer to prevent shunting through back contact – negligible contribution to performance

Why Radial Junction Solar Cells?

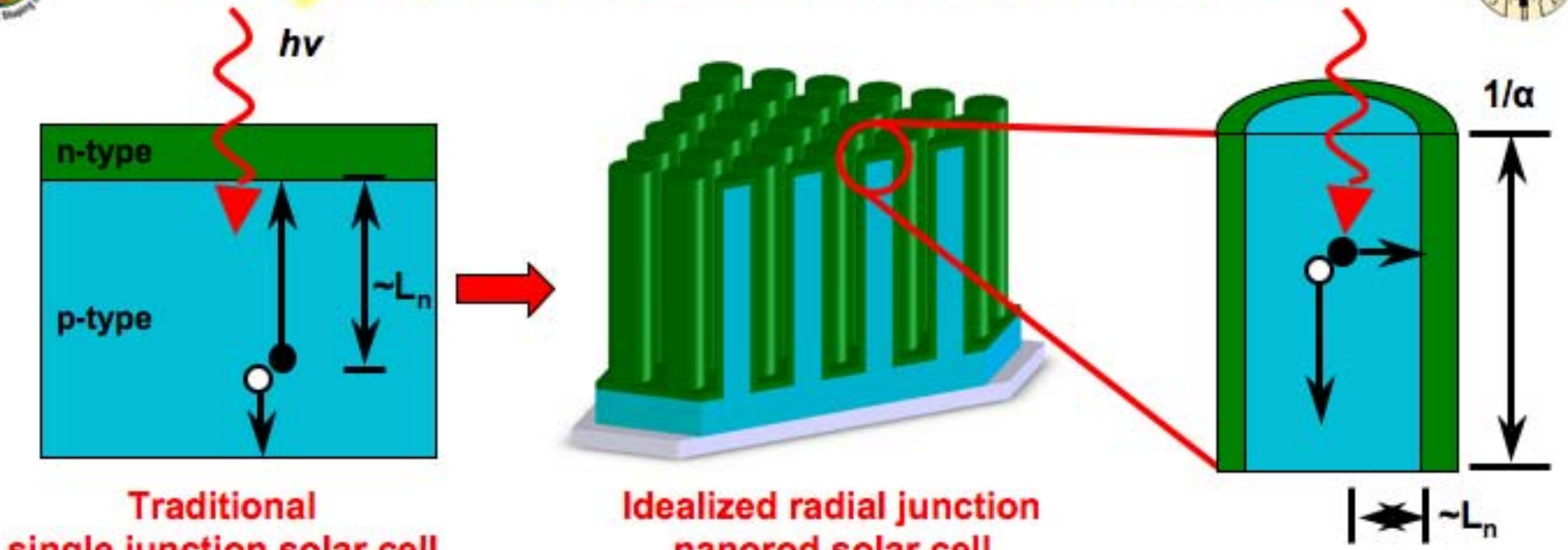

- Traditional device design requires long minority carrier diffusion lengths, and therefore expensive materials

- **Radial geometry allows for high quantum efficiency despite short minority carrier diffusion lengths**

CdSeTe Nanorods

- Spectral response:

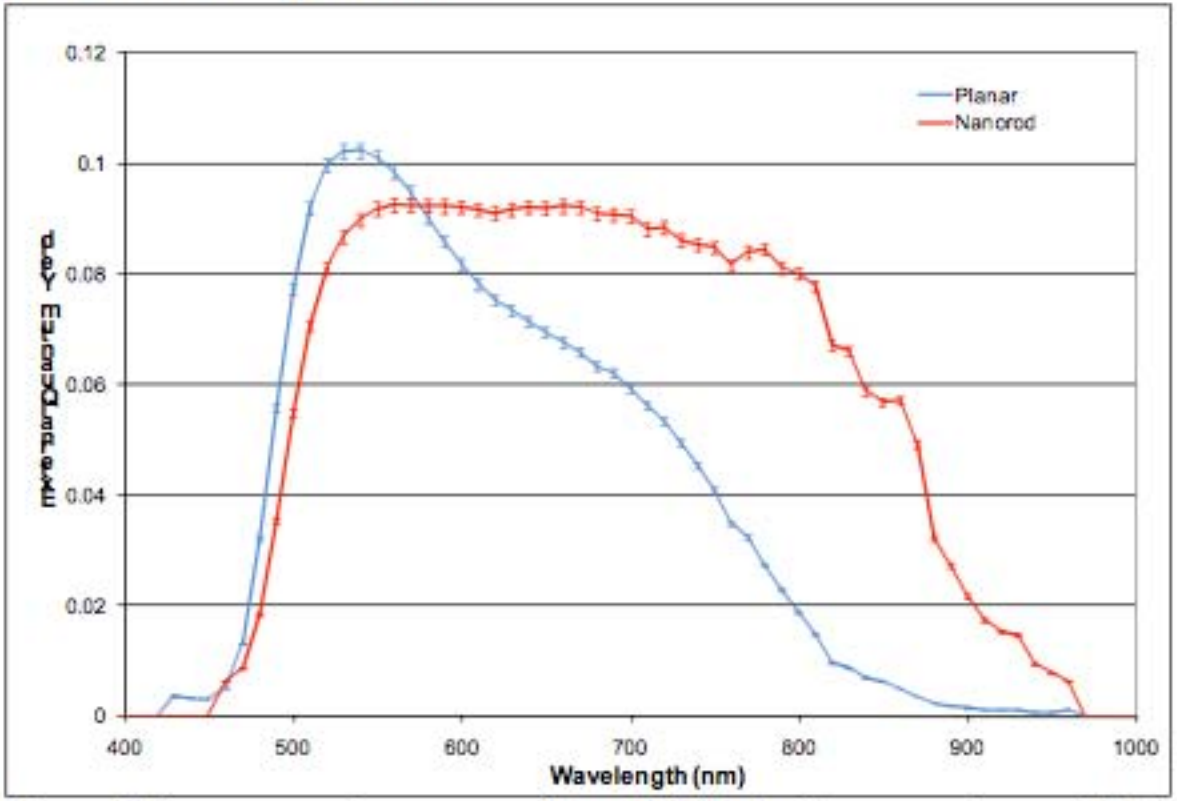

- As expected from IV curves, planar usually exhibits better quantum yields – the above curves were chosen because their similar magnitudes allow for ease of shape comparison
- Shape of the curve is more significant
  - Nanorod samples lose less **quantum yield in the red**
  - Since longer wavelength light penetrates deeper into the semiconductor, this is an indication that the nanorod geometry is **more effectively collecting the carriers**

Si Nanorods

- Nanorod Array Growth Procedure

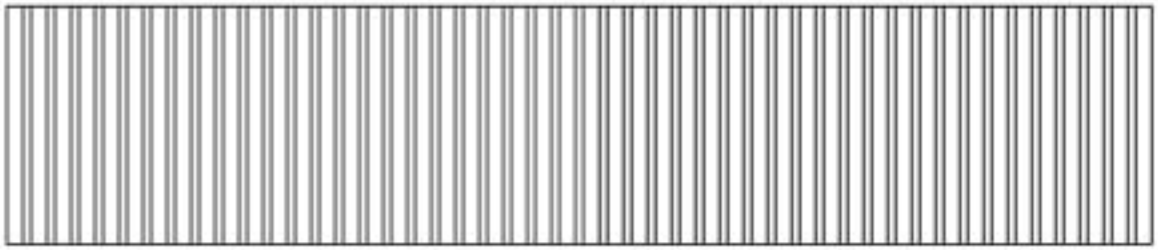

Porous Alumina

Si Nanorods

- Nanorod Array Growth Procedure

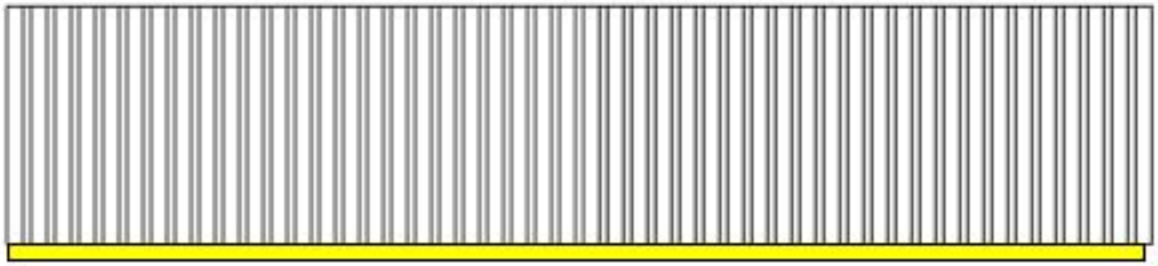

Porous Alumina

Conductive
Catalyst Metal
(via evaporation)

Si Nanorods

- Nanorod Array Growth Procedure

Si Nanorods

- Nanorod Array Growth Procedure

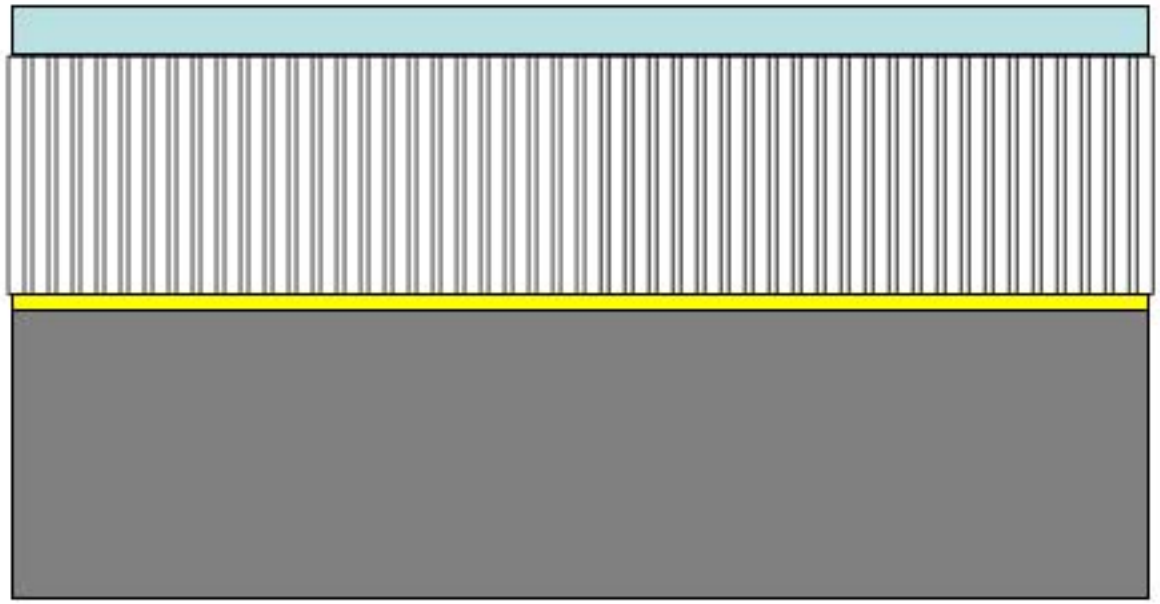

Si Nanorods

- Nanorod Array Growth Procedure

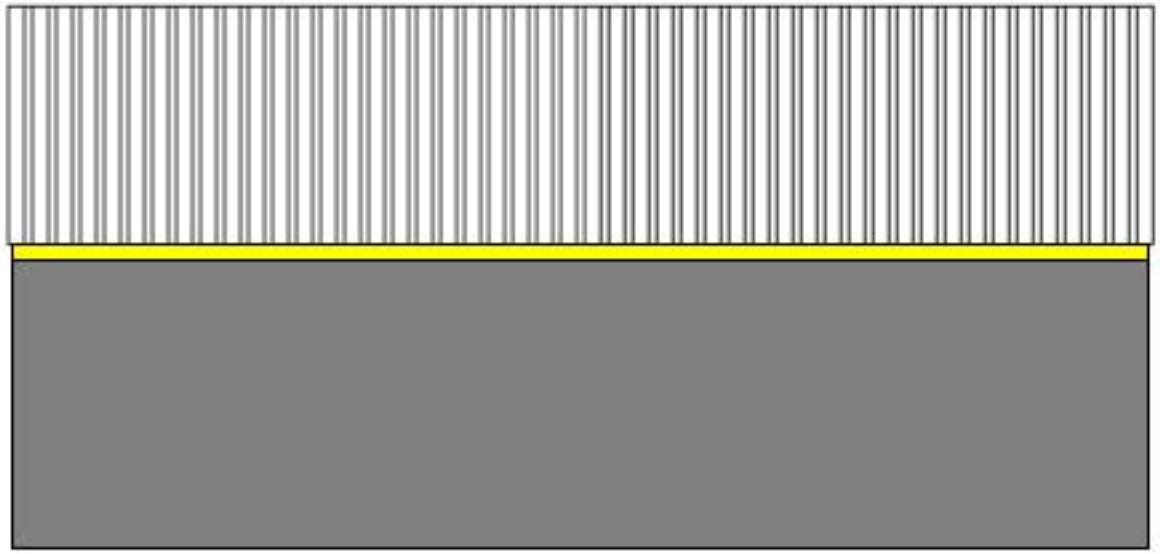

Si Nanorods

- Nanorod Array Growth Procedure

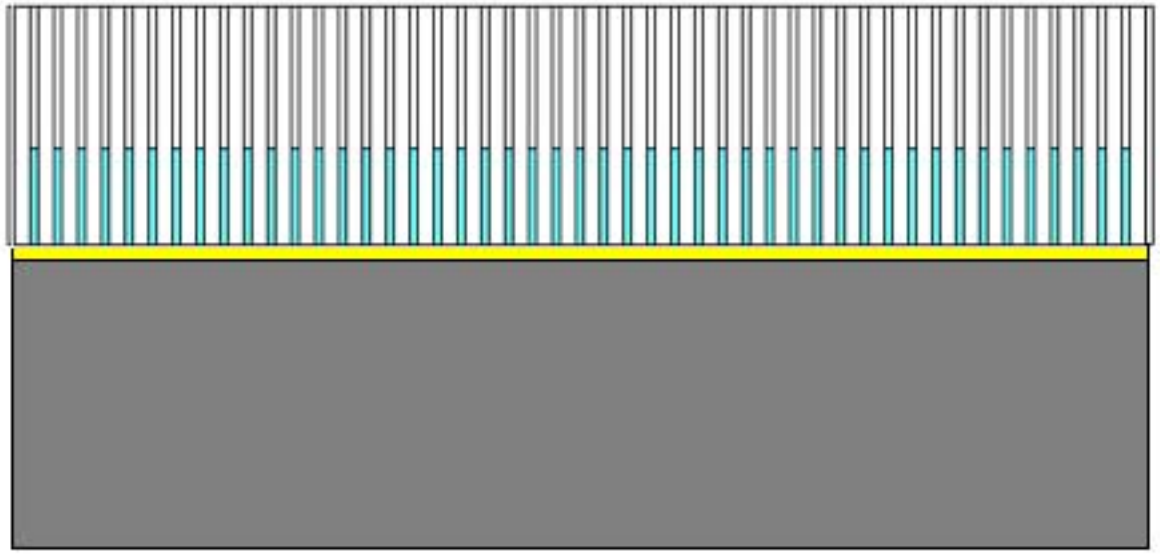

Si Nanorods

- Nanorod Array Growth Procedure

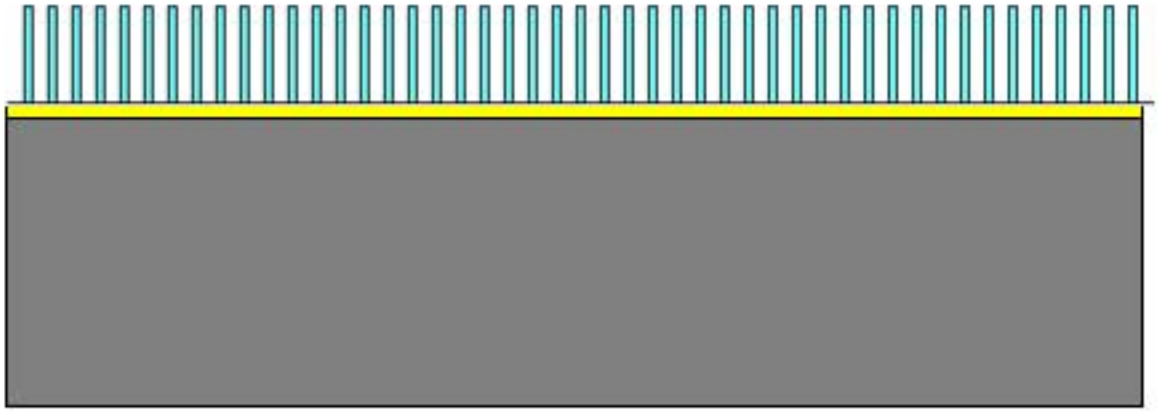

Alumina template removed in 1 M NaOH

Si Nanorods

- Silicon nanorod array after template is removed

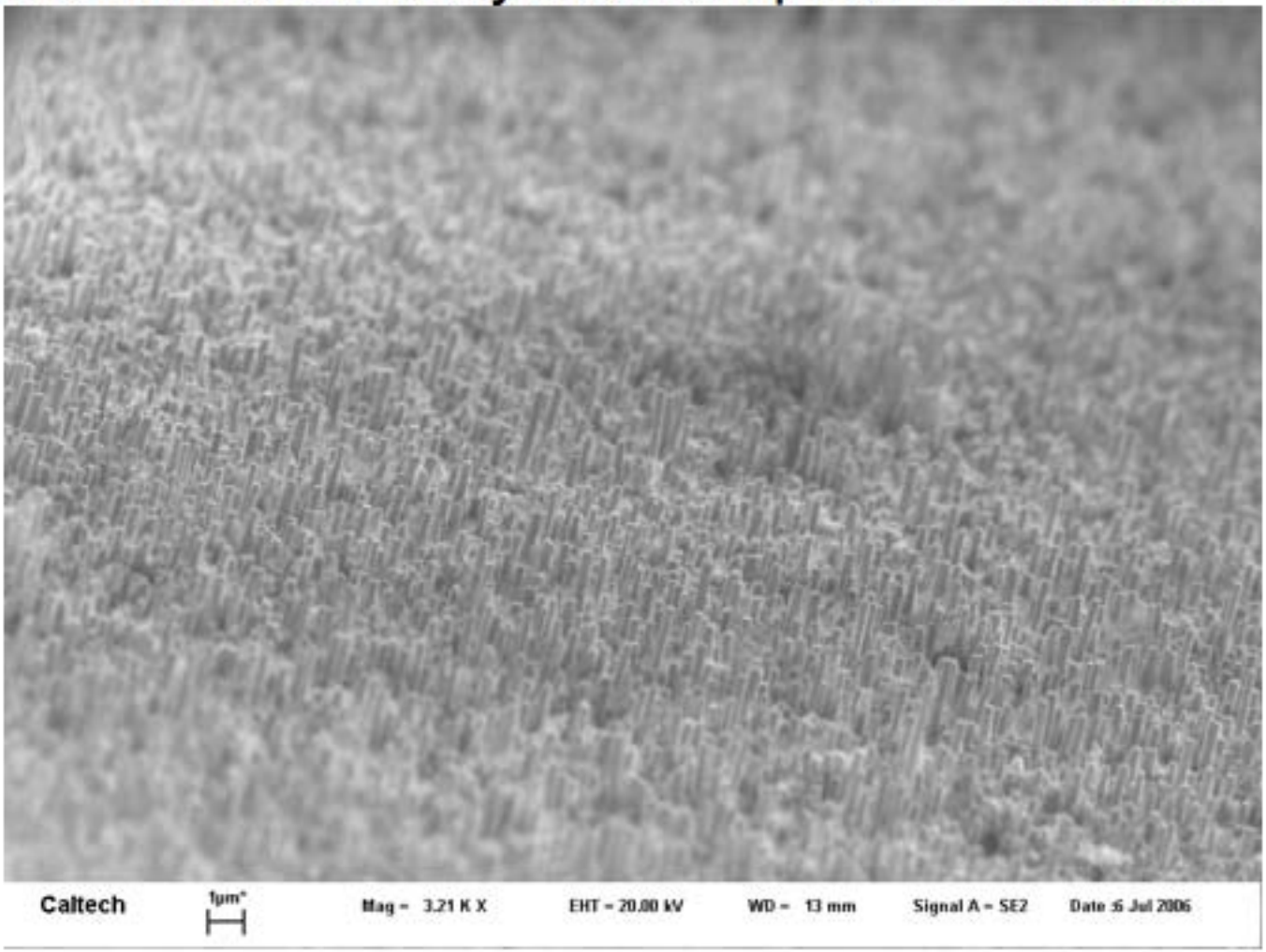

Spatially resolved photocurrent

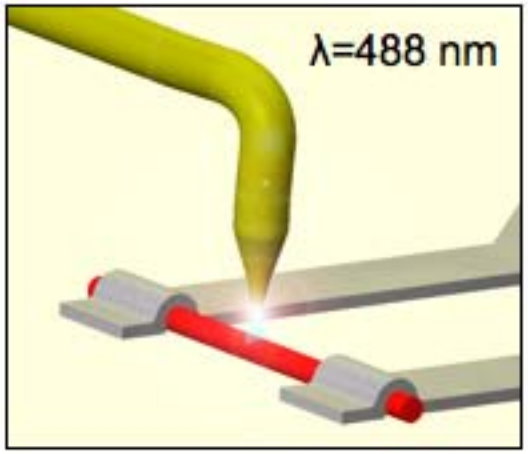

NSOM schematic

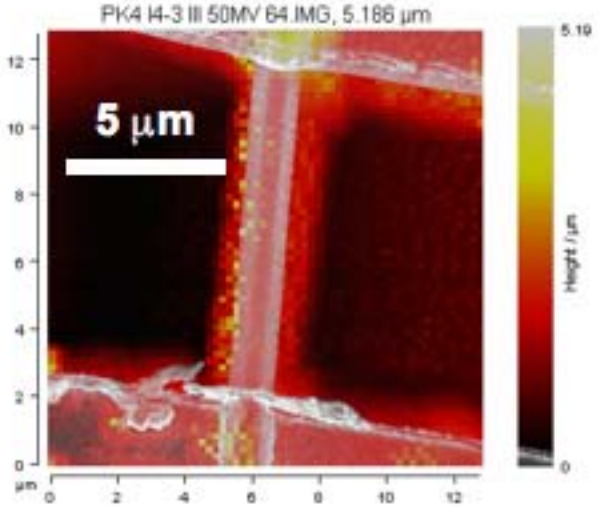

SEM-NSOM Topography Overlay

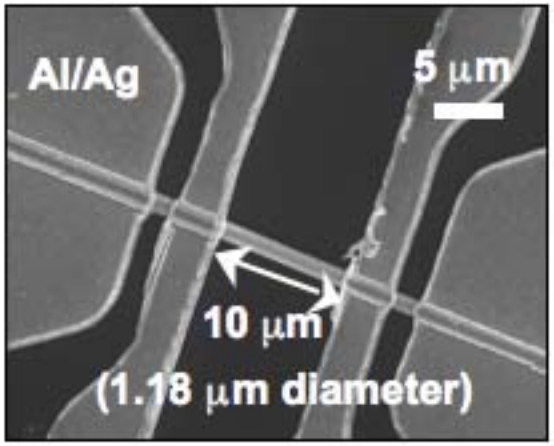

4-Point Probe

- Near-field scanning optical microscopy (NSOM) can measure nanowire photoconductivity as a function of excitation location.
- Carrier collection lengths can be studied as a function of nanowire diameter, growth conditions, passivation, etc...

R_{wire} = 17.9 MΩ

R_C = 200 kΩ

N_D ~ 5×10^{13} cm^{-3}

Effective diffusion length

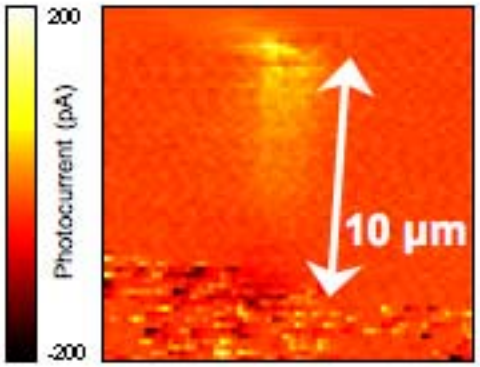

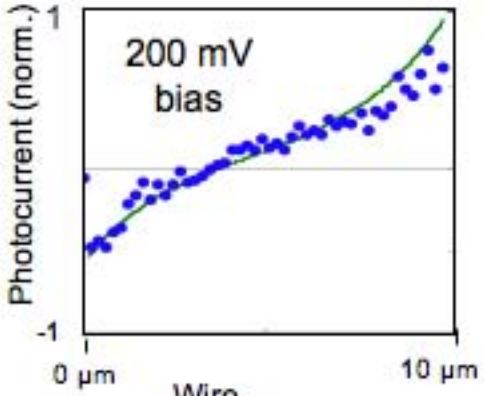

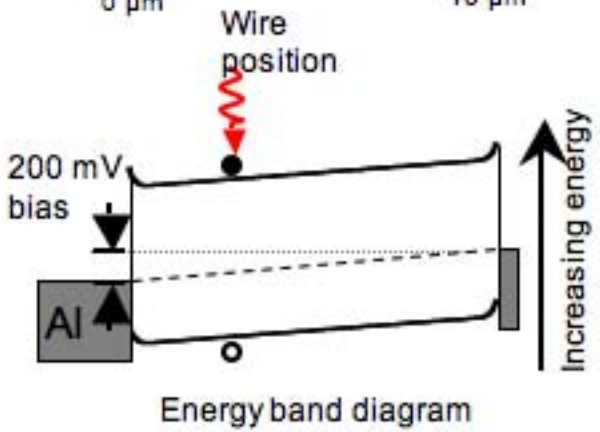

Energy band diagram

Charge transport by drift and diffusion:

$$J_n(x) = q\mu_n n(x)E(x) + qD_n \frac{\partial \delta n}{dx}$$

Charge continuity for electrons with effective, single-τ recombination rate:

$$\frac{\partial \delta n}{\partial t} = \frac{1}{q}\frac{\partial J_n}{\partial x} - \frac{\partial \delta n}{\tau_{n,eff}} + g_n$$

Monitor terminal current as function of injection point:

$$J_{meas} = J_n\,|_{x=0} + J_p\,|_{x=0} \quad \text{when} \quad g_{n,p}\,|_{x=x_{inj}} = I_{ph}$$

Vary τ to match measured photocurrent profile:

$$L_{n,eff} = \sqrt{D_n \tau_{n,eff}} = \mathbf{1.9\ \mu m} \quad \leftrightarrow \quad \tau_{n,eff} \approx 1 \text{ ns}$$

$$L_{p,eff} = \sqrt{D_p \tau_{p,eff}} = \mathbf{2.2\ \mu m} \quad \leftrightarrow \quad \tau_{p,eff} \approx 4 \text{ ns}$$

NSOM suggests minority carrier collection length is comparable to wire diameter.

Oxide Buffer Layer - Pattern Fidelity

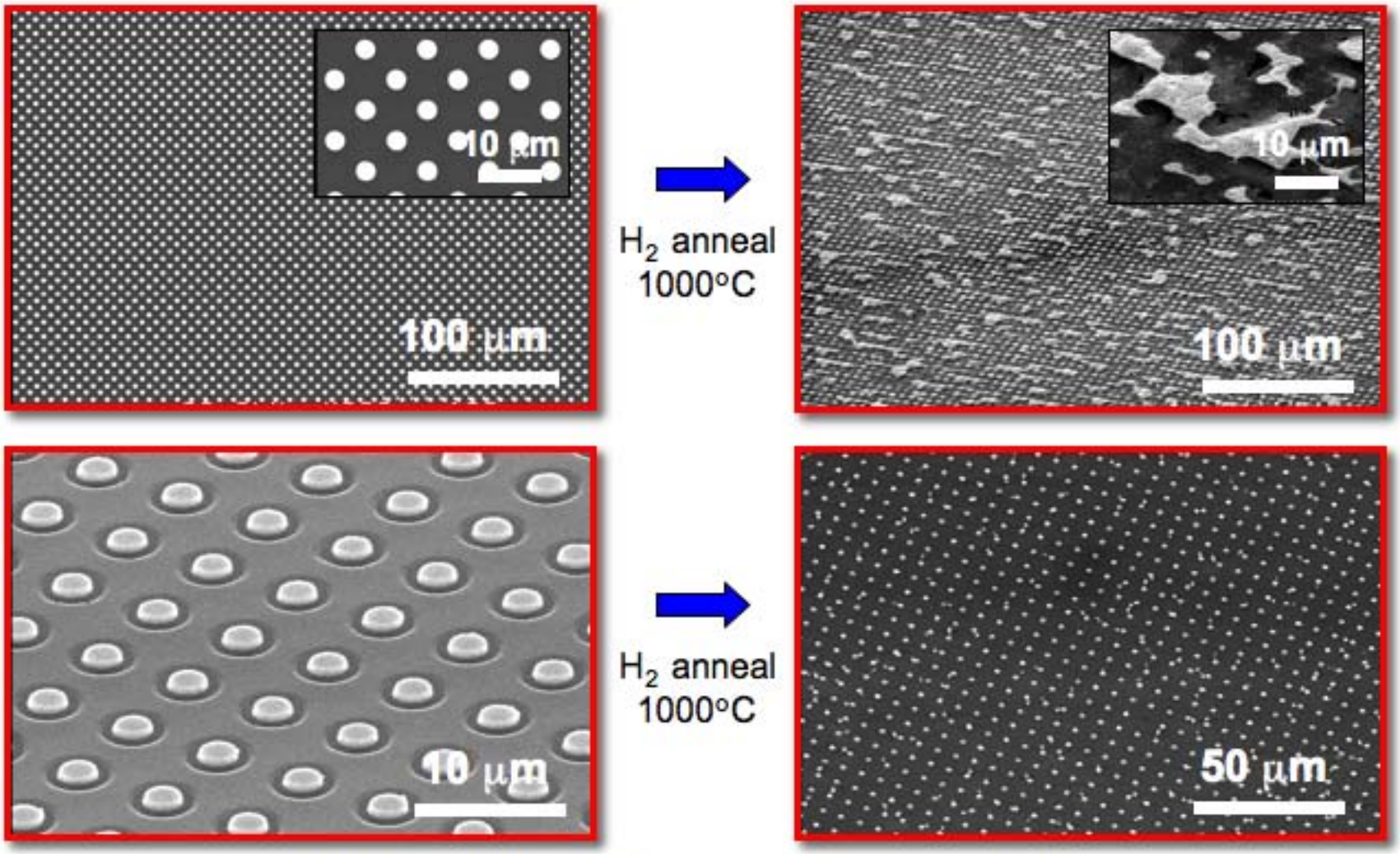

3 μm array, 500 nm Au, T_{growth} = 1000°C, P_{growth} = 760 Torr

An oxide buffer layer is critical for maintaining pattern fidelity during growth.

Large Area Au-Catalyzed Si Arrays

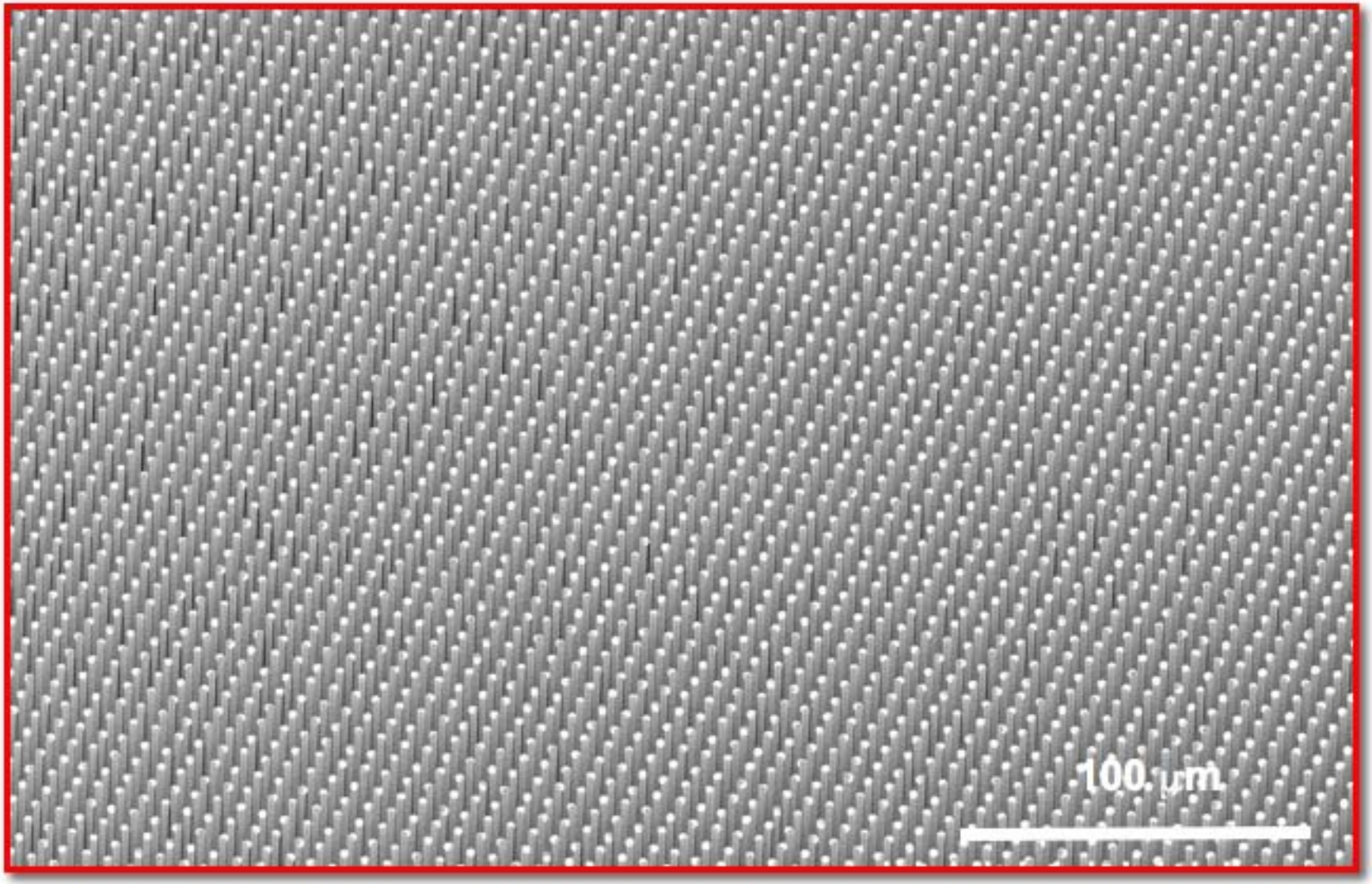

3 μm array, 500 nm Au, T_{growth} = 1000°C, P_{growth} = 760 Torr, 30 min growth, 2 mole % $SiCl_4$ in H_2

Large Area Au-Catalyzed Si Arrays

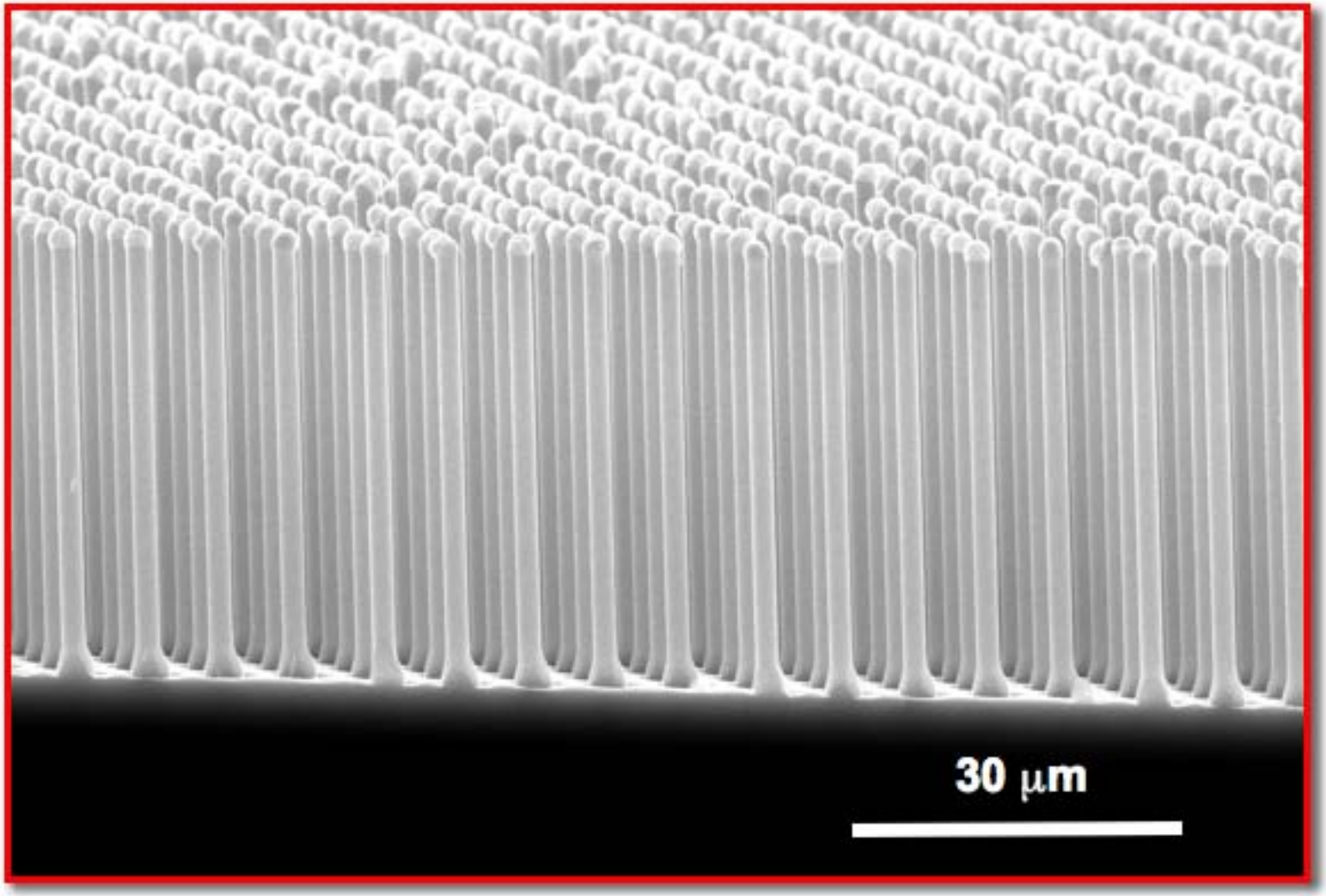

3 μm array, 500 nm Au, T_{growth} = 1000°C, P_{growth} = 760 Torr, 30 min growth, 2 mole % $SiCl_4$ in H_2

Nearly 100% vertically aligned, 75 μm length microwire arrays over areas > 1 cm².

Copper-Catalyzed Si Wire Arrays

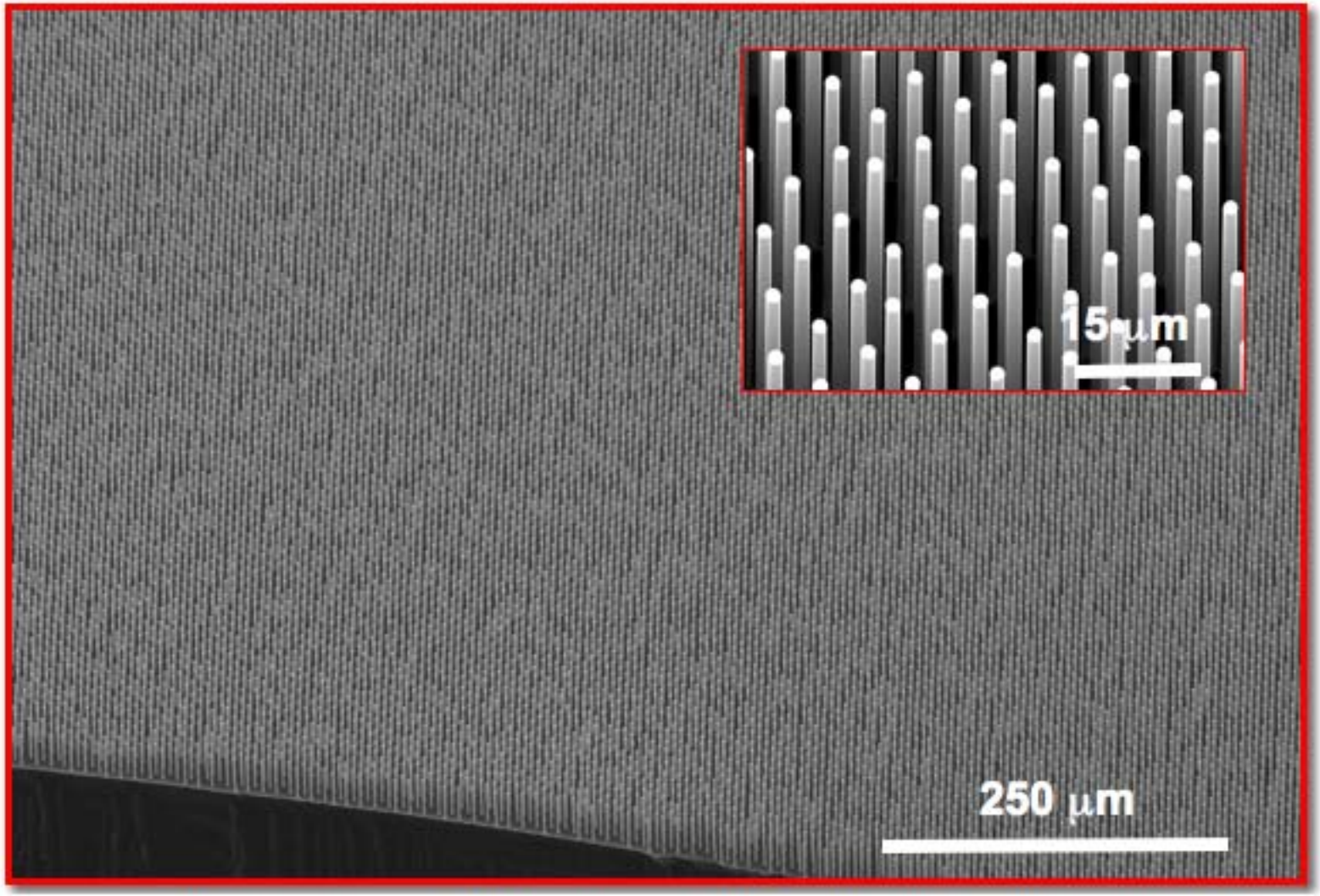

3 μm array, 500 nm Cu, T_{growth} = 1000°C, P_{growth} = 760 Torr, 10 min growth, 2 mole % $SiCl_4$ in H_2

Copper produces wire arrays that are structurally equivalent to gold.

Si Wire Array Junctions

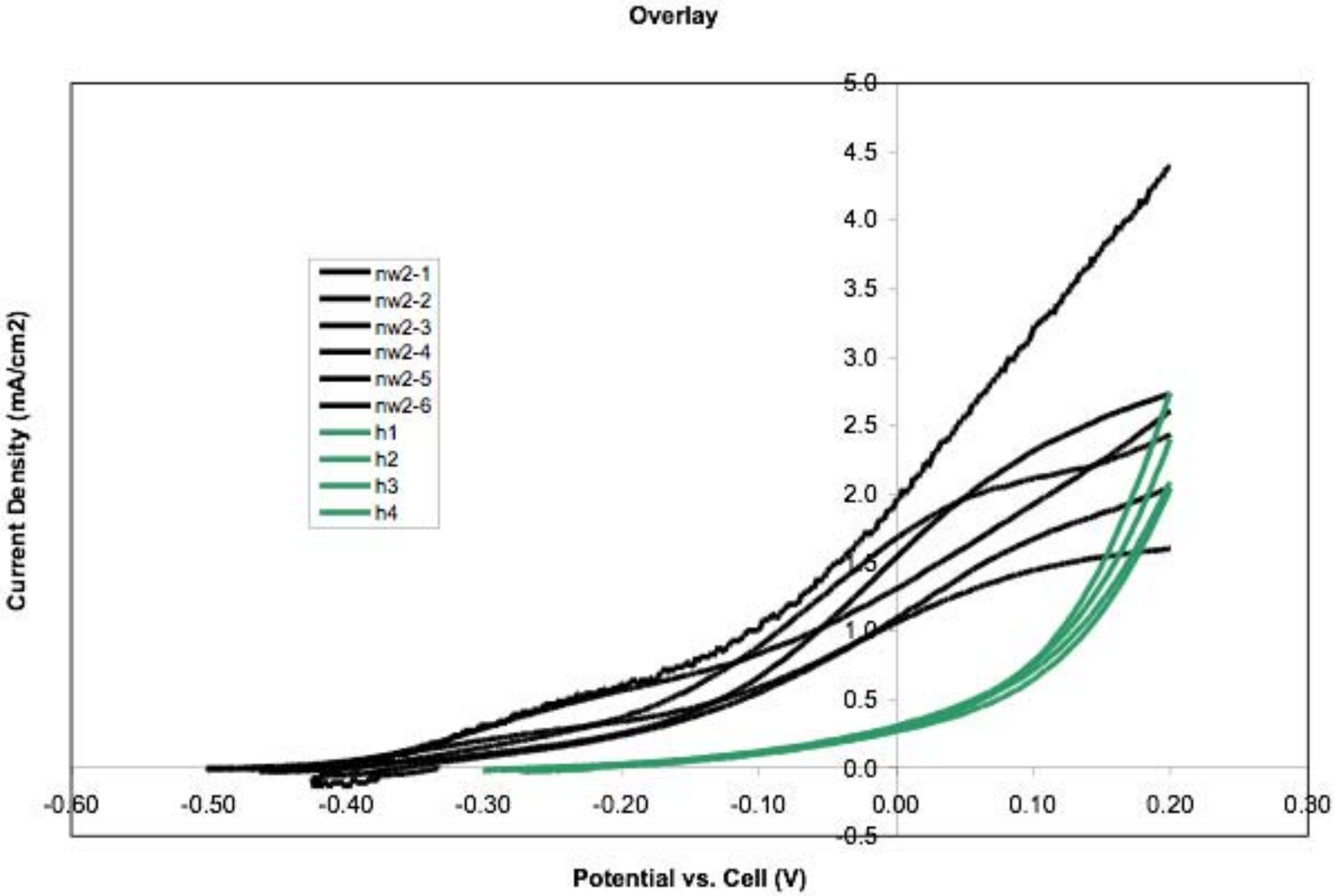

Surface Requirements for Semiconductor Heterojunctions

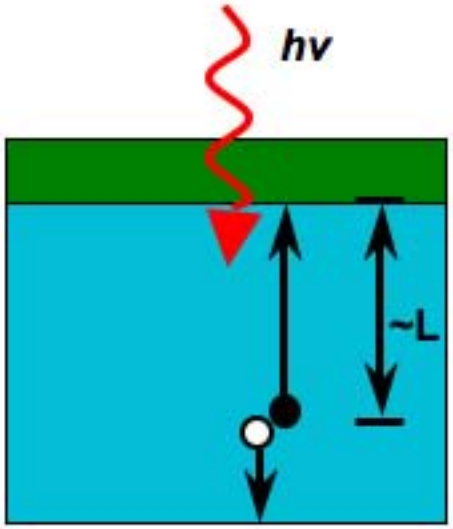

Traditional planar photovoltaic

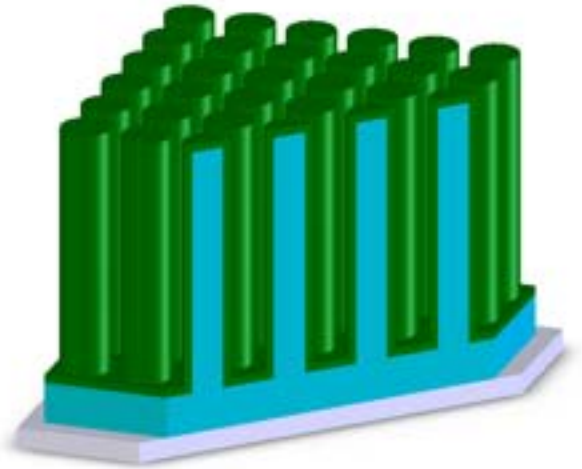

Idealized high aspect ratio photovoltaic

- Low Trap State Density
- Stable in Ambient Conditions
- Facile Interfacial Charge Transfer

Surface Passivation

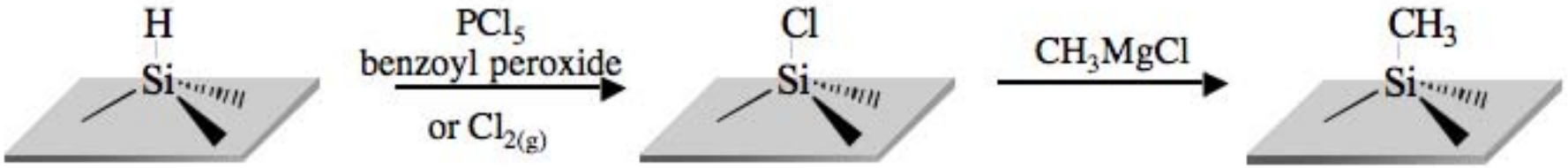

Measured through
STM, $T = 4$ K

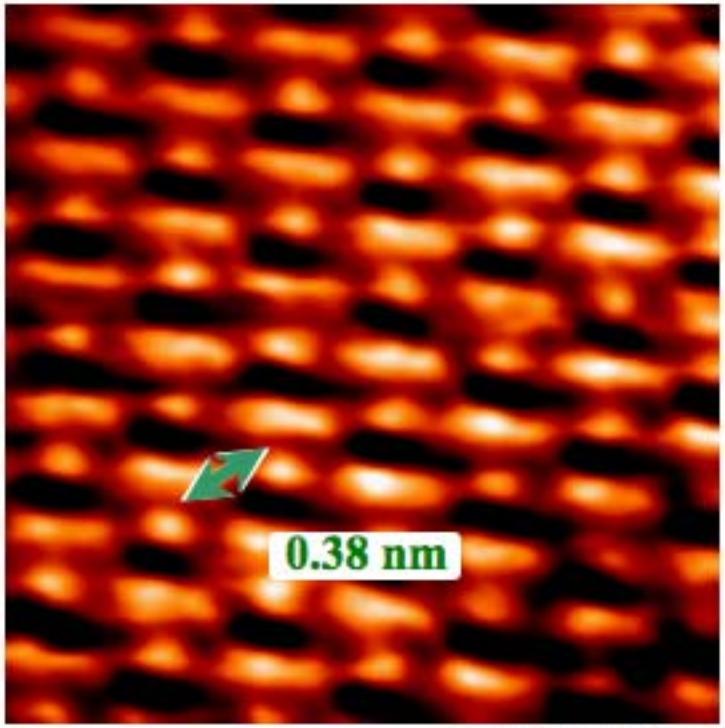

$Si(111)\text{-}CH_3$

SEM of Chlorinated Si Nanorod Arrays

- Chlorination with PCl_5 is known to cause etching of silicon surfaces

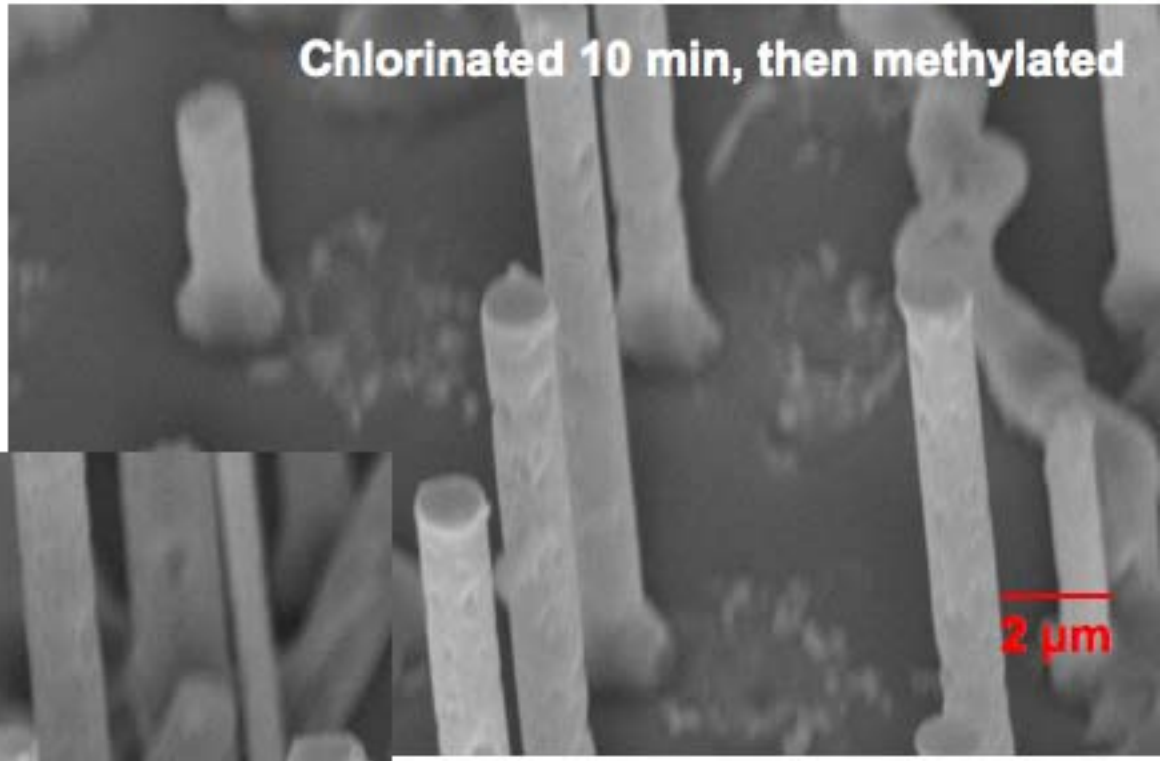

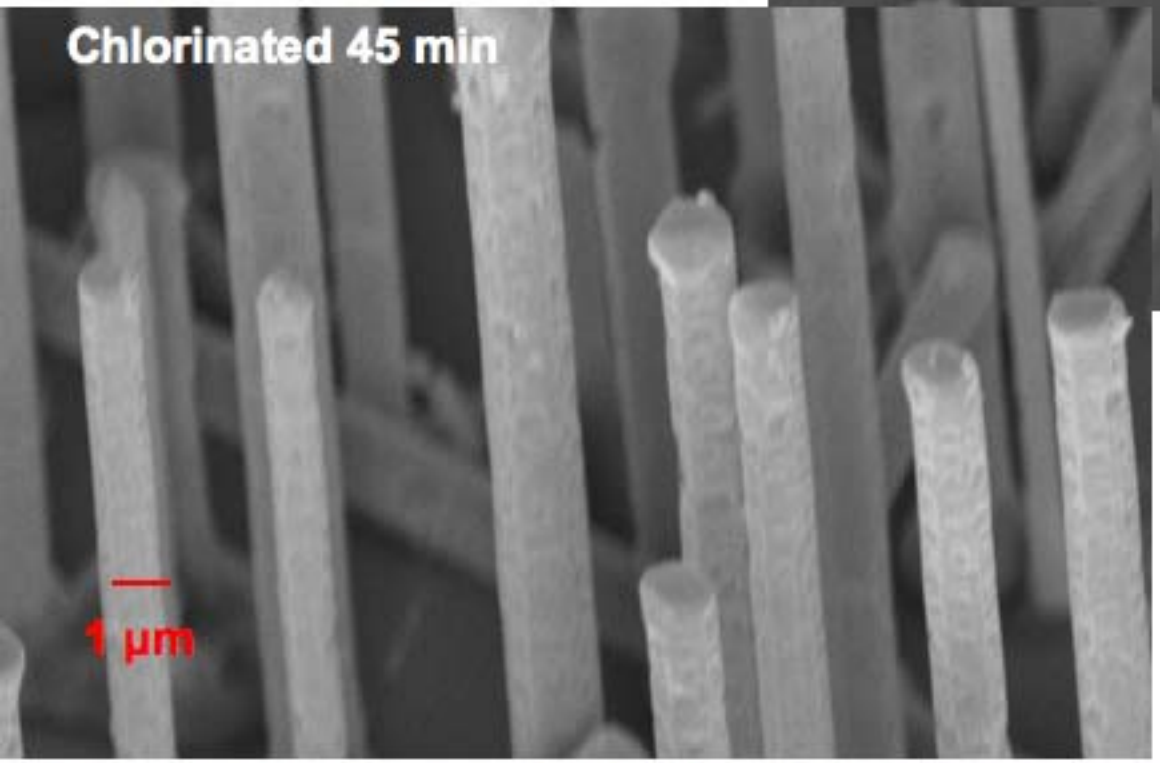

- Functionalized surfaces appear rough, but etching is not destructive

Electrical Performance of Methylated Silicon Nanowires

- Methylated wires (60 nm diameter)
  - Sensitive to gate voltage
  - Maintain higher conductance
- Hydrogen terminated surfaces
  - Deteriorate

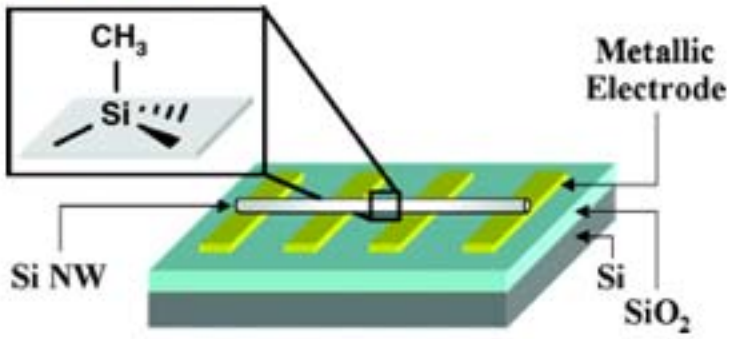

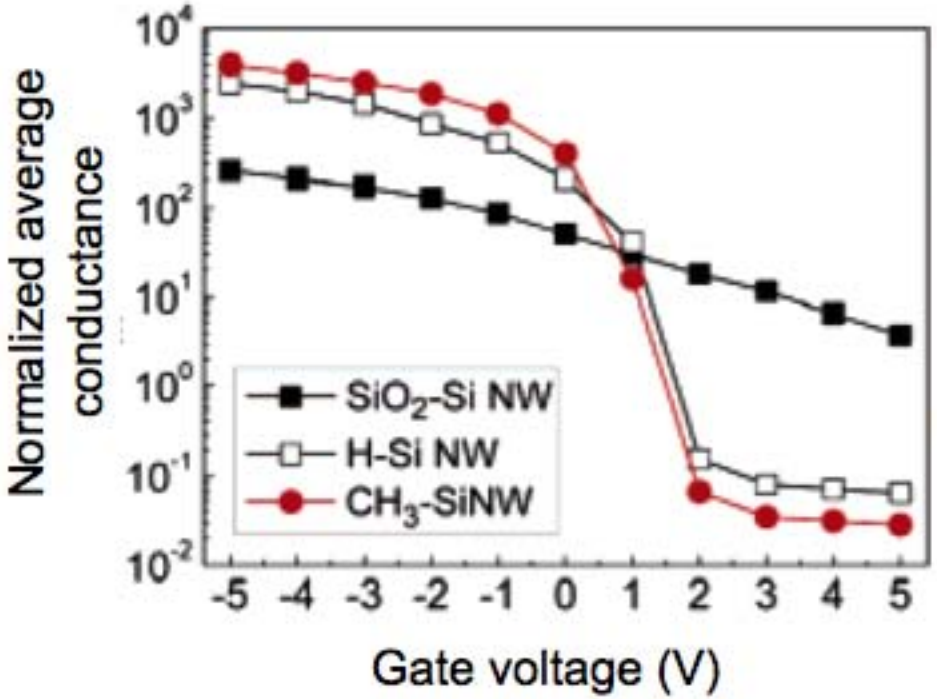

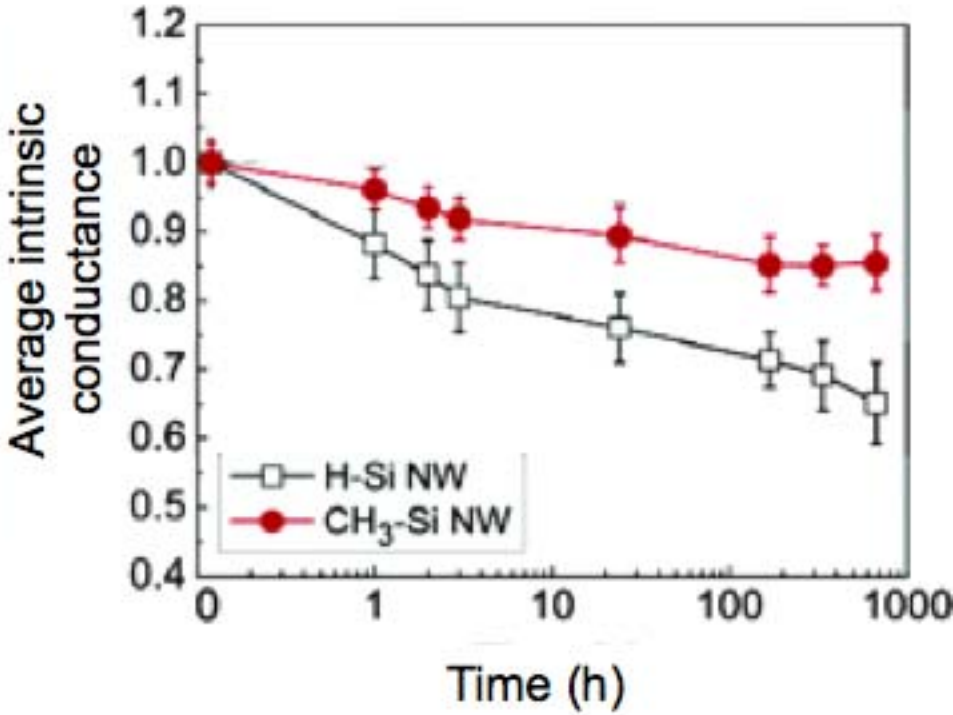

Haick, H.; Hurley, P. T.; Hochbaum, A. I.; Yang, P.; Lewis, N. S. *J. Am. Chem. Soc.* **2006**, *128*, 8990-8991.

Polymerization from Si Rod Surfaces

Allylated Si base

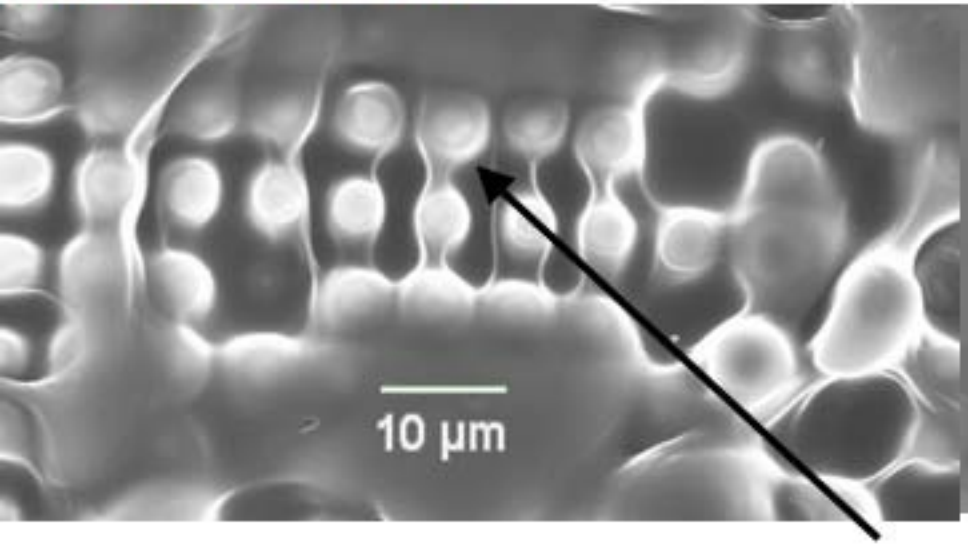

Methylated Si base

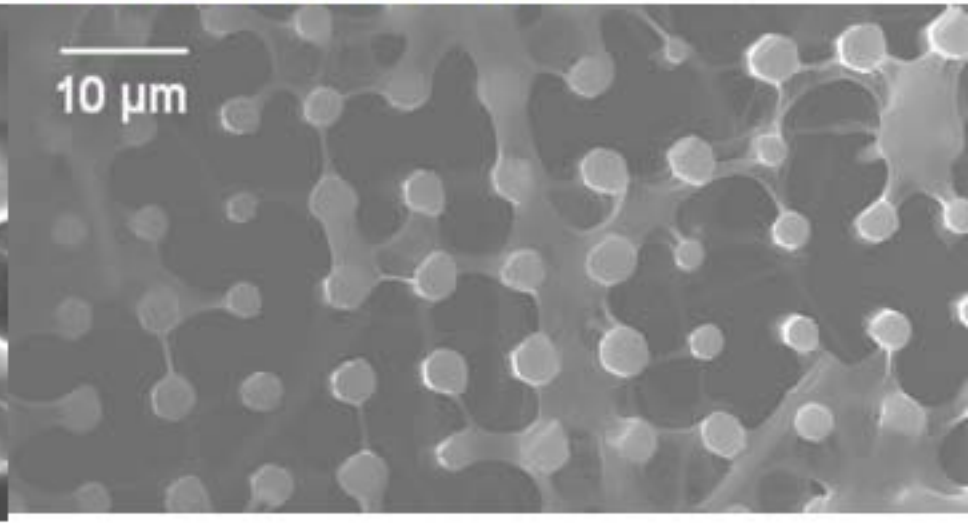

polymer sheath grown around rods!

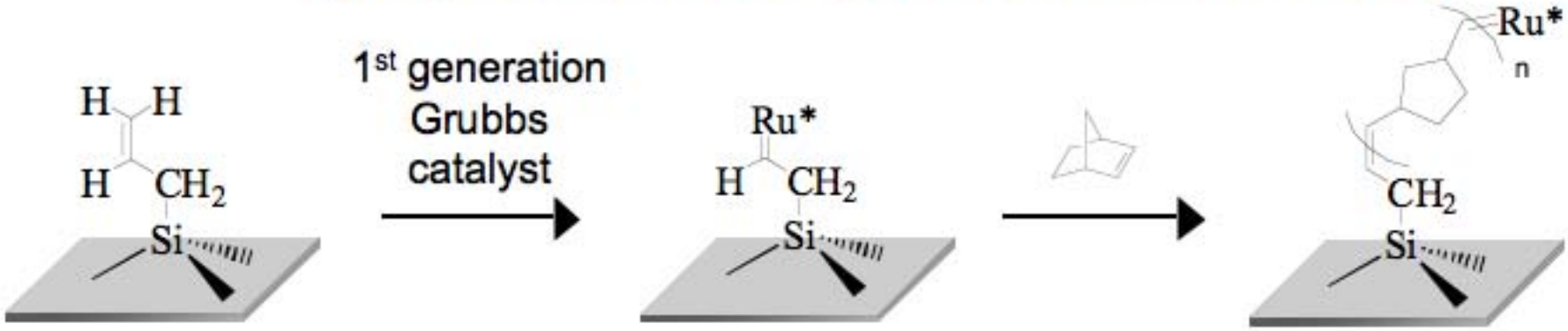

Polymer Embedding of Si Rod Arrays

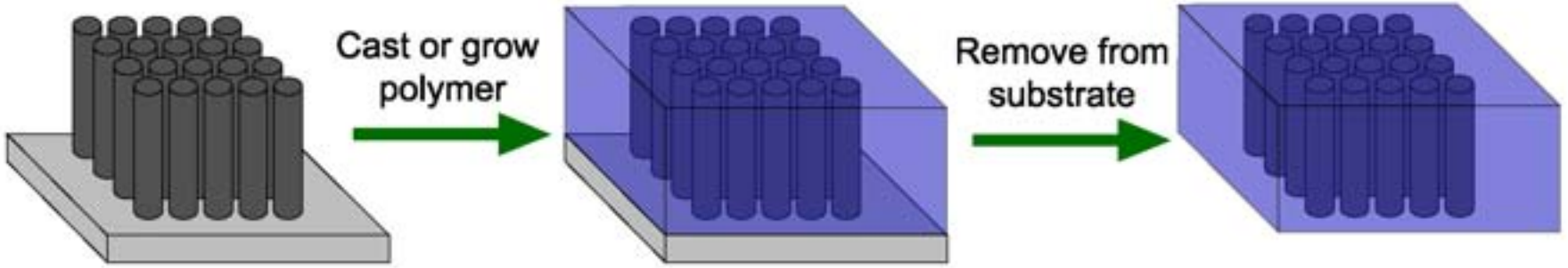

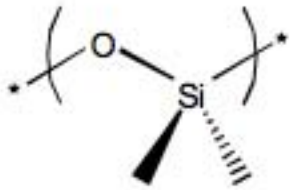

PDMS
(polydimethylsiloxane)

Large Area Rod Array Removal

Top-down view

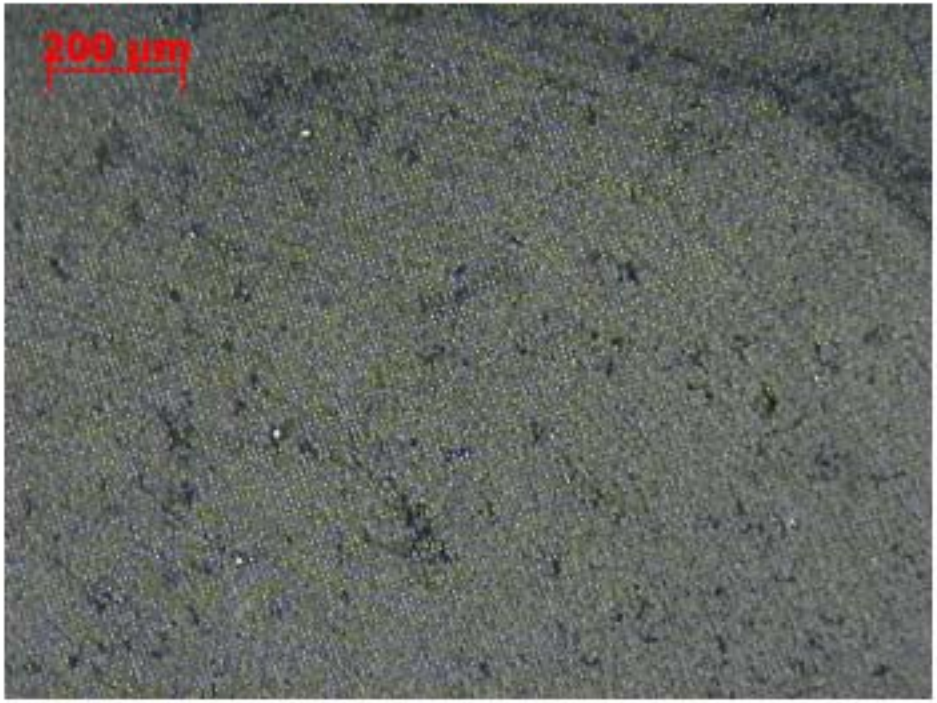

Side view

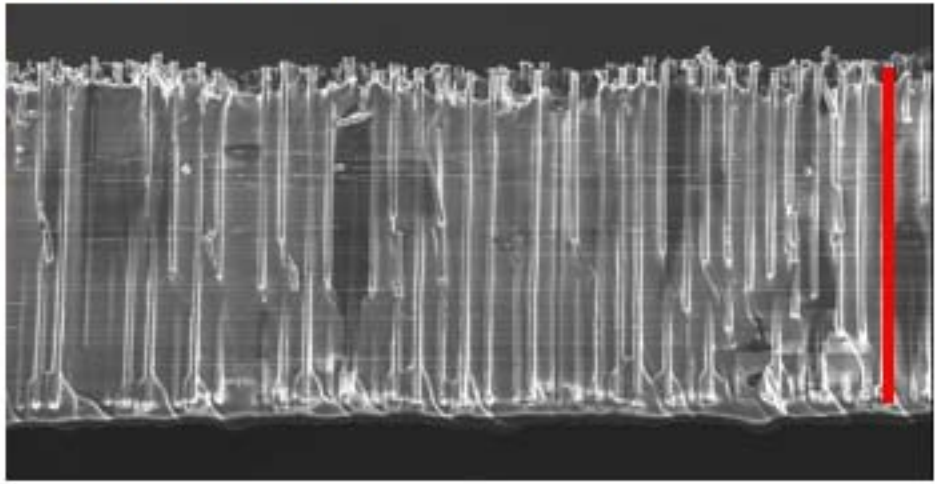

115 µm

- Large area arrays (> 1 cm^2) transferred in one piece.
- Conformal coating from top to bottom of rods

Embedded Rod Pattern Fidelity

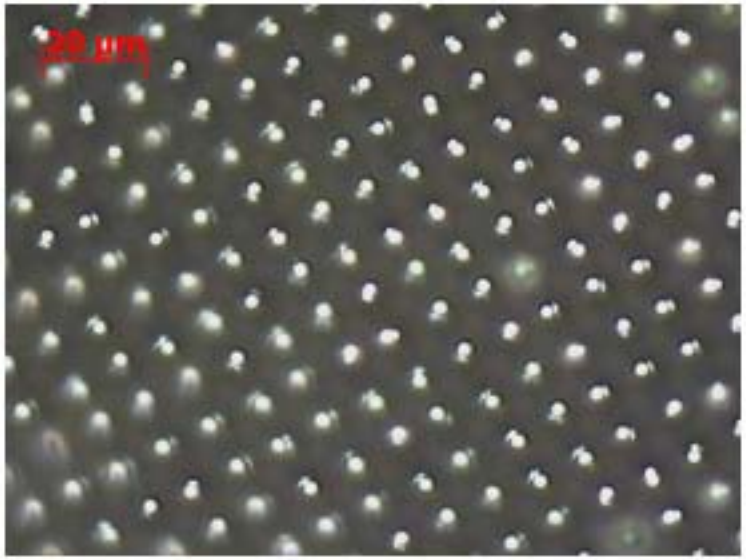

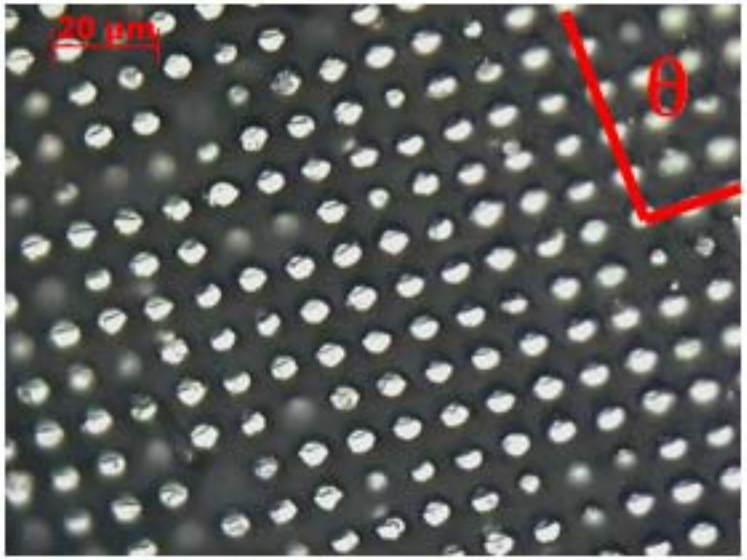

- Inter-rod angle and spacing is constant before and after PDMS casting and removal
- Apparent rod diameter differences due to examination of rod tips versus base

	Rod diameter (μm)	Shortest inter-rod distance (μm)	Angle (θ, °)
Before removal	2.5 ± 2	8.6 ± 2	92 ± 9
After removal	4.6 ± 4	8.8 ± 3	94 ± 2

Dual Junction Nanorod Arrays

- 1.23 V needed to electrolyze water
- Requires a heterojunction or dual junction
- Single absorber: band gap of 2.0-2.6 eV that straddles the necessary potentials
- Photoanode and photocathode absorbers:

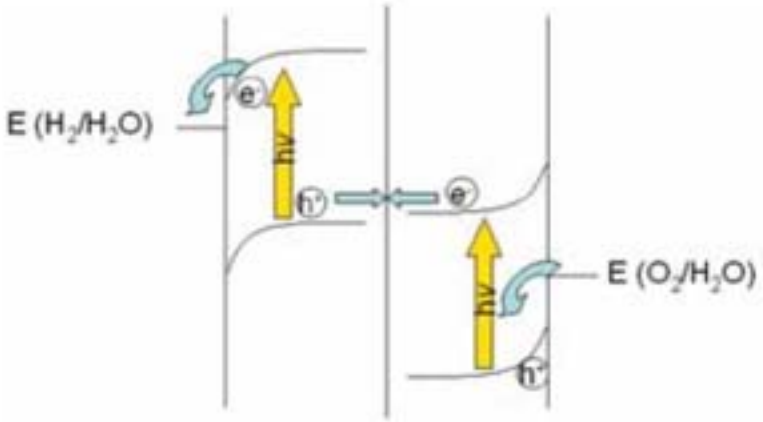

  Band gaps can better match the solar spectrum (1.1-1.4 eV)

  Allows for greater flexibility in materials design

  Efficiency could approach 25%

- Optimal structure would have several light-absorbing layers absorbing different portions of the spectrum with an overall potential greater than 1.23 V

Fe_2O_3 Nanowires

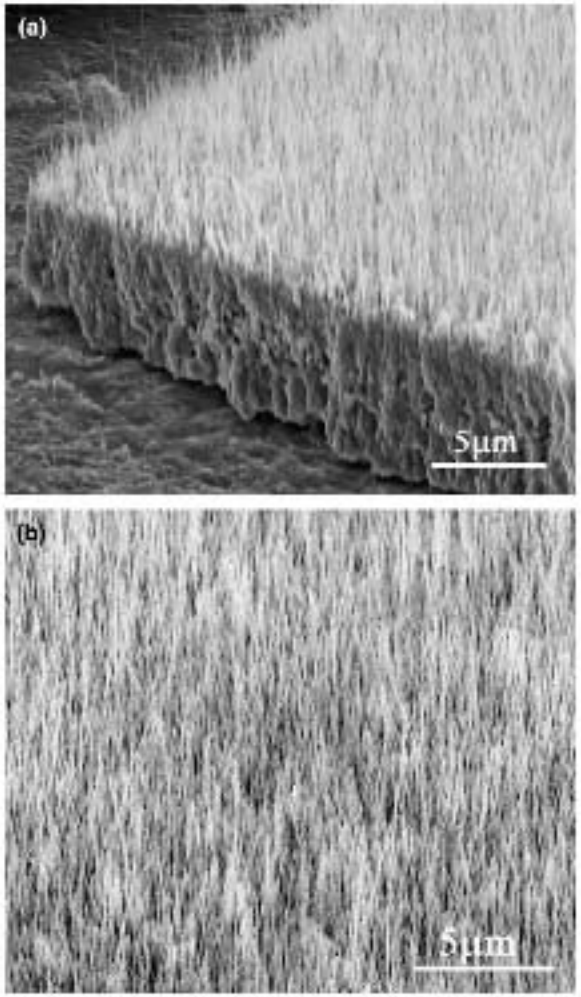

System Concept

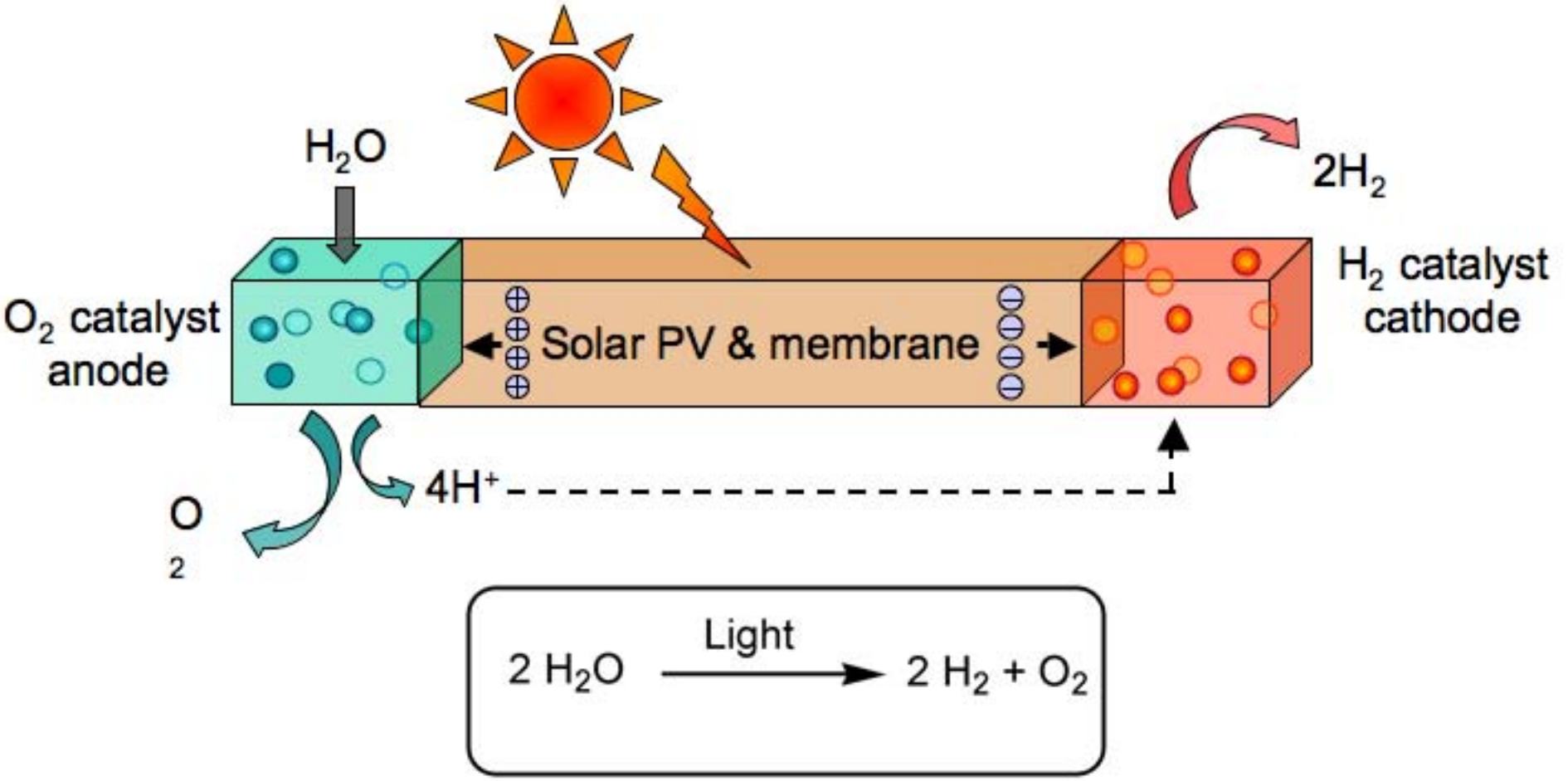

Conclusions

- Without **massive** quantities (10-20 TW by 2050) of clean energy, CO_2 levels will continue to rise
- The only sufficient supply-side cards we have are "clean" coal, nuclear fission (with a closed fuel cycle), and/or cheap solar fuel
- We need to pursue globally scalable systems that can efficiently and cost-effectively capture, convert, and store sunlight in the form of chemical fuels
  - He that can not store, will not have power after four
- Semiconductor/liquid junctions offer the *only* proven method for achieving this goal, but we have a great deal of fundamental science to learn to enable the underpinnings of a cost-effective, deployable technology
  - Nanorods, randomly ordered junctions to generate the needed potential
  - Catalysts to convert the incipient electrons into fuels by rearranging the chemical bonds of water (and CO_2) into O_2 and a reduced fuel